MULTI-SCALE HYPERGRAPH MEETS LLMS: ALIGNING LARGE LANGUAGE MODELS FOR TIME SERIES ANALYSIS

Anonymous authors
Paper under double-blind review

ABSTRACT

Recently, there has been great success in leveraging pre-trained large language models (LLMs) for time series analysis. The core idea lies in effectively aligning the modality between natural language and time series. However, the multi-scale structures of natural language and time series have not been fully considered, resulting in insufficient utilization of LLMs capabilities. To this end, we propose MSH-LLM, a **M**ulti-**S**cale **H**ypergraph method that aligns **L**arge **L**anguage **M**odels for time series analysis. Specifically, a hyperedging mechanism is designed to enhance the multi-scale semantic information of time series semantic space. Then, a cross-modality alignment (CMA) module is introduced to align the modality between natural language and time series at different scales. In addition, a mixture of prompts (MoP) mechanism is introduced to provide contextual information and enhance the ability of LLMs to understand the multi-scale temporal patterns of time series. Experimental results on 27 real-world datasets across 5 different applications demonstrate that MSH-LLM achieves the state-of-the-art results. Code is available at: https://anonymous.4open.science/r/MSH-LLM-1E9B.

1 INTRODUCTION

Time series analysis is a critical ingredient in a myriad of real-world applications, e.g., forecasting (Liu et al., 2023b; Wan et al., 2024; Shang et al., 2024a), imputation (Wang et al., 2024a), and classification (Chen et al., 2024b; Wang et al., 2024c), which is applied across diverse domains, including retail, transportation, economics, meteorology, healthcare, etc. In these real-world applications, the task-specific models usually require domain knowledge and custom designs (Chen et al., 2024a; Zhou et al., 2023a). This contrasts with the demand of time series foundation models, which are designed to perform well in diverse applications, including few-shot learning and zero-shot learning, where minimal and no training data is provided.

Recently, pre-trained foundation models, especially large language models (LLMs), have achieved great success across many fields, e.g., natural language processing (NLP) (Touvron et al., 2023; Achiam et al., 2023; Radford et al., 2021) and computer vision (CV) (Wang et al., 2024b; Pi et al., 2024). Although the lack of large pre-training datasets and a consensus unsupervised objective makes it difficult to train foundation models for time series analysis from scratch (Sun et al., 2024; Jin et al., 2024; Pan et al., 2024), the fundamental commonalities between natural language and time series in sequential structure and contextual dependency provide an avenue to apply LLMs for time series analysis. The core idea lies in the effective alignment of the modality between natural language and time series, either by reprogramming the input time series (Xue & Salim, 2023; Cao et al., 2024) or by introducing prompts to provide contextual information for the input time series (Sun et al., 2024; Kamarthi & Prakash, 2023; Jin et al., 2024).

In the process of aligning LLMs for time series analysis, we observe that both natural language and time series present multi-scale structures. In natural language, multi-scale structures typically manifest as semantic structures at different scales (Yang et al., 2024b), e.g., words, phrases, and sentences. In time series, the multi-scale structures often demonstrate as multi-scale temporal patterns (Wen et al., 2021; Liu et al., 2021; Shang et al., 2024a). For example, due to periodic human activities, traffic occupation and electricity consumption show clear daily patterns (e.g., afternoon or evening) and weekly patterns (e.g., weekday or weekend). Considering multi-scale alignment

between natural language and time series enables models to learn richer representations and enhance their cross-modality learning abilities. However, we argue that performing multi-scale alignment is a non-trivial task, as two notable problems need to be addressed.

The first problem lies in the disparity between the multi-scale semantic space of natural language and that of time series. The multi-scale semantic space of natural language is both distinctive and informative (Pan et al., 2024), while the multi-scale semantic space of time series faces the semantic information sparsity problem due to an individual time point containing less semantic information (Shang et al., 2024b; Chang et al., 2024). This disparity makes it difficult to leverage off-the-shelf LLMs for time series analysis. To tackle this, most existing works employ patch-based methods (Nie et al., 2022; Jin et al., 2024) to capture group-wise interactions and enhance the semantic information of time series semantic space. However, simple partitioning of patches may introduce noise interference and make it hard to discover implicit interactions.

The second problem when performing multi-scale alignment lies in the knowledge and reasoning capabilities to interpret temporal patterns are not naturally present within the pre-trained LLMs. To unlock the knowledge within LLMs and activate their reasoning capabilities for time series analysis, existing methods introduce prefix prompts (Jin et al., 2024; Liu et al., 2024) or self-prompt mechanisms (Sun et al., 2024) to provide task instruction and enrich the input contextual information. While these methods are intuitive and straightforward, they struggle to understand temporal patterns due to their failure to leverage multi-scale temporal features. Therefore, it is still an open challenge to design prompts that are accurate, data-correlated, and task-specific.

Motivated by the above, we propose MSH-LLM, a **M**ulti-**S**cale **H**ypergraph method that aligns **L**arge **L**anguage **M**odels for time series analysis. To the best of our knowledge, MSH-LLM is the first multi-scale alignment work for time series analysis, which leverages the hyperedging mechanism to enhance the multi-scale semantic information of time series and employs the mixture of prompts mechanism to enhance the ability of LLMs in understanding multi-scale temporal patterns. The main contributions of this paper are summarized as follows:

- We introduce a hyperedging mechanism that leverages learnable hyperedges to extract hyperedge features with group-wise information from multi-scale temporal features, which can enhance the multi-scale semantic information of time series semantic space while reducing irrelevant information interference.
- We design a cross-modality alignment module to perform multi-scale alignment based on the multi-scale prototypes and hyperedge features, which goes beyond relying solely on single-scale alignment and obtains richer representations. In addition, we propose a mixture of prompts (MoP) mechanism, which augments the input contextual information with different prompts to enhance the reasoning ability of LLMs for time series analysis.
- We conduct experiments on 27 real-world datasets across 5 different applications. The experimental results demonstrate that MSH-LLM achieves the state-of-the-art (SOTA) performance, highlighting its effectiveness in activating the capability of LLMs for time series analysis.

2 Related Work

In-Modality Learning Methods. Recent studies in NLP (Devlin, 2018; Radford et al., 2019; Brown, 2020; Touvron et al., 2023) and CV (Touvron et al., 2021; Wang et al., 2023; Bao et al., 2022) have shown that pre-trained foundation models can be fine-tuned for various downstream tasks within the same modality, significantly reducing the need for costly training from scratch while maintaining high performance. BERT (Devlin, 2018) uses bidirectional encoder representations from transformers to recover the random masked tokens of the sentences. GPT3 (Brown, 2020) trains a transformer decoder on a large language corpus with much more parameters, which can be utilized for diverse applications. BEiT (Bao et al., 2022) designs a masked image modeling task to pretrain vision transformers. Motivated by the above, recent time series pre-trained models use different strategies, e.g., supervised learning methods (Fawaz et al., 2018) or self-supervised learning methods (Chen et al., 2025; Woo et al., 2022a), to learn representations across diverse domains and then fine-tune on similar applications to perform specific tasks. However, due to the lack of large pre-training datasets and a consensus unsupervised objective, it is difficult to train foundation models for general-purpose time series analysis that covers diverse applications.

Cross-Modality Learning Methods. Due to the fundamental commonalities between natural language and time series in sequential structure and contextual dependency, recent works have explored cross-modality learning by applying LLMs for time series analysis (Bian et al., 2024; Zhou et al., 2023a; Liu et al., 2024; Jin et al., 2024). FPT (Zhou et al., 2023a) is the pilot work that fine-tunes the key parameters of LLMs and transforms them into a unified framework for time series analysis. aLLM4TS (Bian et al., 2024) introduces a two-stage pre-training strategy that first performs causal next-patch training and then enacts a fine-tuning strategy for downstream tasks. However, fine-tuning LLMs for training and inference can sometimes be resource-consuming due to the immense size of LLMs (Liu et al., 2024). Some recent works have explored the alignment of frozen LLMs for time series analysis, either by reprogramming the input time series or introducing prompts to provide contextual information for the input time series. Time-LLM (Jin et al., 2024) introduces a reprogramming mechanism to align the input time series with text prototypes before feeding it into the frozen LLMs. AutoTimes (Liu et al., 2024) repurposes frozen LLMs as autoregressive time series forecasters and introduces relevant time series prompts to enhance forecasting. Although these methods achieve promising results, they overlook the multi-scale structures of natural language and time series.

Multi-Scale Time Series Analysis Methods. Existing multi-scale time series analysis methods are aimed at modeling temporal pattern interactions at different scales (Chen et al., 2021; Shang et al., 2024b; Chen et al., 2023). TAMS-RNNs (Chen et al., 2021) disentangles input series into multi-scale representations and uses different update frequencies to model multi-scale temporal pattern interactions. Benefiting from the attention mechanism, transformers achieve promising results in time series analysis. Pyraformer (Liu et al., 2021) treats multi-scale features as nodes and leverages pyramidal attention to model interactions between nodes at different scales. To solve the problem of semantic information sparsity, Pathformer (Chen et al., 2023) divides time series into multiple resolutions using patches of different sizes and uses the dual attention to capture group-wise pattern interactions at different scales. MSHyper (Shang et al., 2024b) combines transformer with multi-scale hypergraphs to model group-wise pattern interactions at different scales. However, fixed segments or pre-defined rules cannot capture implicit pattern interactions and may introduce noise interference.

In this paper, we find that both natural language and time series present multi-scale structures. Therefore, we propose a multi-scale hypergraph method that aligns large language models (LLMs) for time series analysis. Specifically, a hyperedging mechanism is introduced to enhance the multi-scale semantic information of time series semantic space and reduce noise interference. Then, a cross-modality alignment (CMA) module is introduced to perform multi-scale alignment. In addition, a mixture of prompts (MoP) mechanism is designed to enhance the reasoning capabilities of LLMs towards the multi-scale temporal patterns.

3 PRELIMINARIES

Hypergraph. A hypergraph can be represented as $\mathcal{G} = \{\mathcal{V}, \mathcal{E}\}$, where $\mathcal{V} = \{v_1, \ldots, v_n, \ldots, v_N\}$ denotes the node set and $\mathcal{E} = \{e_1, \ldots, e_m, \ldots, e_M\}$ denotes the hyperedge set. Each hyperedge represents group-wise interactions by connecting a set of nodes $\{v_1, v_2, \ldots, v_n\} \subseteq \mathcal{V}$. The topology of the hypergraph can be represented by the incidence matrix $\mathbf{H} \in \mathbb{R}^{N \times M}$, where $\mathbf{H}_{nm} = 1$ if the nth node connected to the mth hyperedge, otherwise $\mathbf{H}_{nm} = 0$. The degree of the nth node is defined as $d(v_n) = \sum_{m=1}^{M} \mathbf{H}_{nm}$ and the degree of the mth hyperedge is defined as $d(v_m) = \sum_{n=1}^{N} \mathbf{H}_{nm}$. The node degrees and hyperedge degrees are sorted in diagonal matrices $\mathbf{D}_{\mathrm{v}} \in \mathbb{R}^{N \times N}$ and $\mathbf{D}_{\mathrm{e}} \in \mathbb{R}^{M \times M}$, respectively. More descriptions of hypergraph learning are provided in Appendix C.

Problem Definition. The proposed MSH-LLM is designed to align frozen LLMs for time series analysis, which covers different applications across various domains. For a given specific application that consists the input time series $\mathbf{X}^{\mathrm{I}}_{1:T} \in \mathbb{R}^{T \times D}$ with T time steps and D dimensions, the goal of time series analysis is to predict important properties of the time series. For example, the forecasting task aims at predicting the future H steps $\mathbf{X}^{\mathrm{O}}_{T+1:T+H} \in \mathbb{R}^{H \times D}$, while the classification task aims at predicting the class labels of the given time series.

4 METHODOLOGY

As depicted in Figure 1, MSH-LLM focuses on reprogramming an embedding-visible large language model, e.g., LLaMA (Touvron et al., 2023) and GPT-2 (Radford et al., 2019), for general time series analysis, while accounting for the multi-scale structures of natural language and time series.

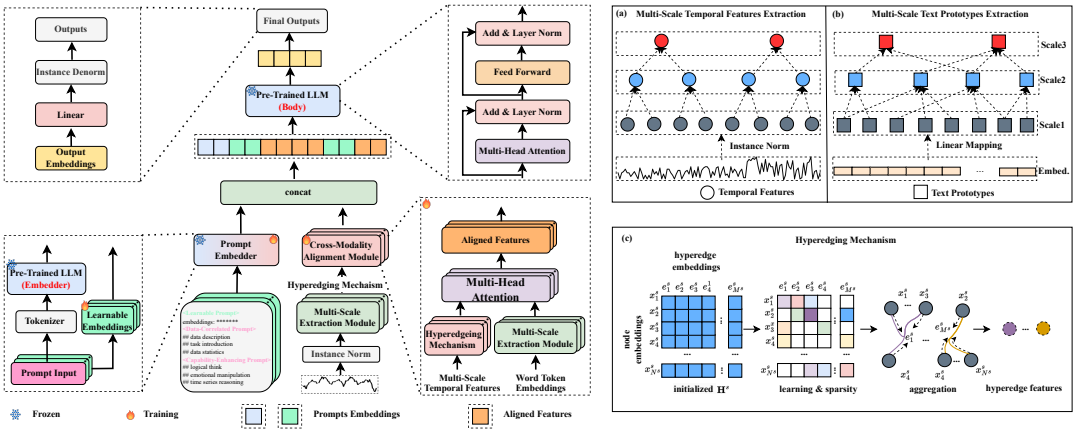

Figure 1: The framework of MSH-LLM. (a) and (b) provide detailed delineation of the multi-scale extraction module, while (c) elaborates on the hyperedging mechanism.

In doing so, we first map the time series data and word token embeddings (based on pre-trained LLMs) into multi-scale temporal features and text prototypes, respectively. Then, a hyperedging mechanism is designed to enhance the multi-scale semantic information of time series semantic space and a cross-modality alignment (CMA) module is introduced to align the modality between natural language and time series. In addition, a mixture of prompts (MoP) mechanism is introduced to provide multi-scale contextual information and enhance the ability of LLMs in understand multi-scale temporal patterns of time series.

4.1 Multi-Scale Extraction (ME) Module

The ME module is designed to extract the multi-scale features, which includes multi-scale temporal features extraction and multi-scale text prototypes extraction.

Multi-Scale Temporal Features Extraction. As shown in Figure 1(a), given input time series $\mathbf{X}^1 = \mathbf{X}^{\mathrm{I}}_{1:T}$, we first normalize it through reversible instance normalization (Kim et al., 2021). Then, we perform multi-scale temporal features extraction, which can be formulated as follows:

$$\mathbf{X}^s = Agg(\mathbf{X}^{s-1}; \theta^{s-1}) \in \mathbb{R}^{N^s \times D}, s \geq 2, \tag{1}$$

where $\mathbf{X}^s = \{\boldsymbol{x}^s_t | \boldsymbol{x}^s_t \in \mathbb{R}^D, t \in [1, N^s]\}$ denotes the sub-sequence at scale s, $s = 2, ..., S$ denotes the scale index, and S is the total number of scales. Agg is the aggregation function, e.g., 1D convolution or average pooling. θ^{s-1} denotes the learnable parameters of the aggregation function at scale $s-1$, $N^s = \left\lfloor \frac{N^{s-1}}{l^{s-1}} \right\rfloor$ is the sequence length at scale s, and l^{s-1} denotes the size of the aggregation window at scale $s-1$.

Multi-Scale Text Prototypes Extraction. The multi-scale text prototypes extraction aims to map word token embeddings in natural language to multi-scale structures, e.g., words, phrases, and sentences, for alignment with multi-scale temporal features. As shown in Figure 1(b), given the word token embeddings based on pre-trained LLMs $\mathbf{U} \in \mathbb{R}^{V \times P}$, where V is the vocabulary size and P is the hidden dimension of LLMs. We first transform them to a small collection of text prototypes through linear mapping, which can be represented as $\mathbf{U}^1 \in \mathbb{R}^{V' \times P}$, where $V' \ll V$. This approach is efficient and can capture key linguistic signals related to time series. Then, we can obtain multi-scale text prototypes through linear mapping, which is formulated as follows:

$$\mathbf{U}^s = Linear(\mathbf{U}^{s-1}; \lambda^{s-1}) \in \mathbb{R}^{V^s \times P}, s \geq 2, \tag{2}$$

where $Linear$ denotes the linear mapping function, $\mathbf{U}^s$ represents the text prototypes at scale s, and λ^{s-1} denotes the learnable parameters of the linear mapping function at scale $s-1$. After mapping, we aim for the multi-scale text prototypes to capture the linguistic signals that describe multi-scale temporal patterns. Experimental results in Appendix H validate the effectiveness of the multi-scale text prototype extraction compared to manually selected approaches.

4.2 HYPEREDGING MECHANISM

After obtaining the multi-scale temporal features and text prototypes, a straight way to align LLMs for time series analysis is to perform cross-modality alignment at different scales. However, the semantic space disparity poses a significant challenge, making it difficult to leverage the off-the-shelf LLMs for time series analysis. To tackle this, some recent studies (Jin et al., 2024; Shang et al., 2024a) show that group-wise interactions can help enrich the semantic information of time series semantic space, thereby enhancing its consistency with the semantic space of natural language. Therefore, we introduce a hyperedging mechanism that utilizes learnable hyperedges to capture group-wise interactions at different scales.

As depicted in Figure 1(c), we first treat multi-scale temporal features as nodes and initialize two kinds of learnable embeddings at scale s, i.e., hyperedge embeddings $\boldsymbol{E}^s_{\text{hyper}} \in \mathbb{R}^{M^s \times D}$ and node embeddings $\boldsymbol{E}^s_{\text{node}} \in \mathbb{R}^{N^s \times D}$, where M^s is a hyperparameter that defines the number of hyperedges at scale s. Then, the similarity calculation is performed to construct the scale-specific incidence matrix $\mathbf{H}^s$, which can be formulated as follows:

$$\begin{aligned} \boldsymbol{U}^s_1 &= tanh(\boldsymbol{E}^s_{\text{nodes}}\boldsymbol{\beta}), \\ \boldsymbol{U}^s_2 &= tanh(\boldsymbol{E}^s_{\text{hyper}}\boldsymbol{\varphi}), \\ \mathbf{H}^s &= Linear(ReLU(\boldsymbol{U}^s_1(\boldsymbol{U}^s_2)^T)), \end{aligned} \tag{3}$$

where $\boldsymbol{\beta} \in \mathbb{R}^{1\times 1}$ and $\boldsymbol{\varphi} \in \mathbb{R}^{1\times 1}$ are learnable parameters. The $tanh$ activation function is used to perform nonlinear transformations and the $ReLU$ activation function is applied to eliminate weak connections. To enhance the robustness of the model, reduce the computation cost of subsequent operations, and mitigate the impact of noise, we introduce a sparsity strategy to make $\mathbf{H}^s$ sparse, which can be formulated as follows:

$$\mathbf{H}^s_{nm} = \begin{cases} 1, & \mathbf{H}^s_{nm} \in TopK(\mathbf{H}^s_{n*}, \eta) \\ 0, & \mathbf{H}^s_{nm} \notin TopK(\mathbf{H}^s_{n*}, \eta) \end{cases} \tag{4}$$

where η is the threshold of $TopK$ function and denotes the max number of neighboring hyperedges connected to a node. The final scale-specific incidence matrices can be represented as $\{\mathbf{H}^1, \cdots, \mathbf{H}^s, \cdots, \mathbf{H}^S\}$ and the hyperedge features of the ith hyperedge $\boldsymbol{e}^s_i \in \boldsymbol{\mathcal{E}}^s$ based on the scale-specific incidence matrix at scale s is formulated as follows:

$$\boldsymbol{e}^s_i = Avg(\sum\nolimits_{\boldsymbol{x}^s_j \in \mathcal{N}(e^s_i)} \boldsymbol{x}^s_j) \in \mathbb{R}^D, \tag{5}$$

where Avg is the average operation, $\mathcal{N}(e^s_i)$ is the neighboring nodes connected by e^s_i at scale s, and $\boldsymbol{x}^s_j \in \mathbf{X}^s$ represents the jth node features at scale s. The final hyperedge feature set at different scales can be represented as $\{\boldsymbol{\mathcal{E}}^1, \cdots, \boldsymbol{\mathcal{E}}^s, \cdots, \boldsymbol{\mathcal{E}}^S\}$.

Compared with other methods, our hyperedging mechanism is novel in two aspects. Firstly, our methods can capture implicit group-wise interactions at different scales in a learnable manner, while most existing methods (Nie et al., 2022; Zhou et al., 2023a; Shang et al., 2024b) rely on pre-defined rules to model group-wise interactions at a single scale. Secondly, although some methods (Shang et al., 2024a; Jiang et al., 2019) learn from hypergraphs, they focus on constraints or clustering-based approaches to learn the hypergraph structures. In contrast, our method learns the hypergraph structures in a data-driven manner by incorporating learnable parameters and nonlinear transformations, which is more flexible and can learn more complex hypergraph structures.

4.3 CROSS-MODALITY ALIGNMENT (CMA) MODULE

The CMA module is designed to align the modality between natural language and time series based on the multi-scale hyperedge features and text prototypes. To achieve this, a multi-head cross-attention is used to perform alignment at different scales. Specifically, for the given text prototpyes $\mathbf{U}^s$ and hyperedge features $\boldsymbol{\mathcal{E}}^s$ at scale s, we first transform it into query $\mathbf{Q}^s_\jmath = \boldsymbol{\mathcal{E}}^s\mathbf{W}^s_{\text{q},\jmath}$, key $\mathbf{K}^s_\jmath = \mathbf{U}^s\mathbf{W}^s_{\text{k},\jmath}$, and value $\mathbf{V}^s_\jmath = \mathbf{U}^s\mathbf{W}^s_{\text{v},\jmath}$, respectively, where $\jmath = 1, ..., \mathcal{J}$ denotes the head index. $\mathbf{W}^s_{\text{q},\jmath} \in \mathbb{R}^{D\times d}$, $\mathbf{W}^s_{\text{k},\jmath} \in \mathbb{R}^{P\times d}$, and $\mathbf{W}^s_{\text{v},\jmath} \in \mathbb{R}^{P\times d}$ are learnable weight matrices at scale s, $d = \lfloor \frac{D}{\mathcal{J}} \rfloor$. Then, the multi-head cross-attention is applied to align the hyperedging features with text prototypes, which

can be formulated as follows:

$$\mathcal{Z}_j^s = Attn(\mathbf{Q}_j^s, \mathbf{K}_j^s, \mathbf{V}_j^s) = softmax(\frac{\mathbf{Q}_j^s(\mathbf{K}_j^s)^\top}{\sqrt{d}})\mathbf{V}_j^s. \tag{6}$$

Then, we aggregate $\mathcal{Z}_k^s$ in every head to obtain the output of multi-head attention $\mathcal{Z}^s \in \mathbb{R}^{M^s \times D}$ at scale s. The final aligned features at different scales can be represented as $\{\mathcal{Z}^1, \cdots, \mathcal{Z}^s, \cdots, \mathcal{Z}^S\}$.

4.4 Mixture of Prompts (MoP) Mechanism

The performance of LLMs depends significantly on the design of the prompts used to steer the model capabilities (Pan et al., 2024; Zhou et al., 2023b). To enhance the reasoning capabilities of LLMs, most existing methods focus on prefix prompts (Jin et al., 2024; Liu et al., 2024) or self-prompt mechanisms (Sun et al., 2024; Lester et al., 2021) to provide task instructions and enrich the input contextual information. However the prompts affecting the reasoning capabilities of LLMs are multifaceted. Relying on a single type of prompt cannot fully activate the reasoning capabilities of LLMs. Therefore, we propose a MoP mechanism, which augments the input contextual information with different prompts (i.e., learnable prompts, data-correlated prompts, and capability-enhancing prompts) and enhances the reasoning capabilities of LLMs towards multi-scale temporal patterns.

Learnable Prompts. Learnable or soft prompts show great effectiveness across many fields by utilizing learnable embeddings, which are learned from the supervised loss between the output of the model and the ground truth. However, existing learnable prompts cannot capture the temporal dynamics from multi-scale temporal patterns. Therefore, we introduce multi-scale learnable prompts $\mathcal{C}_l = \{\mathbf{P}^1, ..., \mathbf{P}^s, ..., \mathbf{P}^S\}$, where $\mathbf{P}^s \in \mathbb{R}^{L^s \times D}$ is the scale-specific prompts and L^s is the prompt length at scale s. $\mathcal{C}_l$ learns from the loss between the output of LLMs and task-specific ground truth.

Data-Correlated Prompts. As shown in Figure 2(a), we introduce three components to construct data-correlated prompts $\mathcal{C}_d$, i.e., data description (π), task introduction (τ), and data statistics (μ). The data description provides LLMs with essential background information about the input time series, the task introduction is used to guide LLMs in understanding and performing specific tasks, and the data statistics provide time series statistics that include both input sequence and sub-sequences at different scales. The final data-correlated prompts can be formulated as follows:

$$\mathcal{C}_d = LLMs(tokenizer(\pi, \tau, \mu)). \tag{7}$$

Capability-Enhancing Prompts. Some recent studies in NLP (Kojima et al., 2022) and CV (Ge et al., 2023) have shown that prompt engineering, e.g., template and chain-of-thought prompts can significantly enhance the reasoning abilities of LLMs, especially for few-shot or zero-shot learning. We have observed the similar rules when aligning LLMs for time series analysis. Therefore, as shown in Figure 2(b), we design three components to construct capability-enhancing prompts $\mathcal{C}_c$, i.e., logical thinking (ϕ), emotional manipulation (φ), and time series reasoning correlated prompts (ψ). The logical thinking prompts guide LLMs to solve problems in a step-by-step manner, which may enhance the multi-step reasoning abilities of LLMs; The emotional manipulation prompts mimic the impact of emotions on human decision-making, using "emotional blackmail" to make the model focus more on the current task; The time series reasoning correlated prompts provide specific methodologies that help LLMs to deal with temporal features. The final capability-enhancing prompts are formulated as follows:

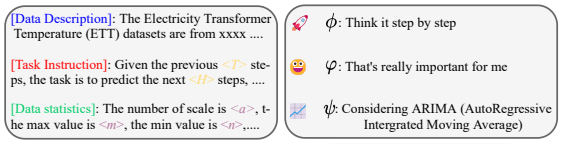

(a) Data-Correlated Prompt (b) Capability-Enhancing Prompt

Figure 2: Prompt example. <> and <> are task-specific configurations and input statistic information, respectively.

$$\mathcal{C}_c = LLMs(tokenizer(\phi, \varphi, \psi)). \tag{8}$$

4.5 Output Projection

After obtaining the MoP, we first concatenate the learnable prompts with the aligned features at different scales, then concatenate it with data-correlated prompts and capability-enhancing prompts and put them into LLMs to get the output representations, which can be formulated as follows:

$$\mathcal{O} = LLMs([\mathcal{C}_d, \mathcal{C}_c, [\mathbf{P}^1, \mathcal{Z}^1], ..., [\mathbf{P}^S, \mathcal{Z}^S]]). \tag{9}$$

where $[.,.]$ denotes the concatenation operation. Then, we obtain the final results through linear mapping and instance denormalization.

5 EXPERIMENTS

Experimental Settings. We conduct experiments on 27 real-world datasets across 5 different applications to verify the effectiveness of MSH-LLM, including long/short-term time series forecasting, classification, few-shot learning, and zero-shot learning. Overall, MSH-LLM achieves state-of-the-art results in a range of critical time series analysis tasks against 19 adavanced baselines. More details about baselines, datasets, and experiment settings are given in Appendix B, D, and E, respectively.

5.1 LONG-TERM FORECASTING

Setups. For long-term time series forecasting, we evaluate the performance of MSH-LLM on 7 commonly used datasets, including ETT (i.e., ETTh1, ETTh2, ETTm1, and ETTm2), Weather, Traffic, and Electricity datasets. More details about the datasets are given in Appendix D. Following existing works (Jin et al., 2024; Zhou et al., 2023a; Pan et al., 2024), we set the input length $T = 512$ and the forecasting lengths $H \in \{96, 192, 336, 720\}$. The mean square error (MSE) and mean absolute error (MAE) are set as the evaluation metrics.

Table 1: Long-term time series forecasting results. Results are averaged from all forecasting lengths. Lower values mean better performance. The best results are **bolded** and the second best results are underlined. Full results are listed in Appendix G.1, Table 11.

Methods	MSH-LLM (Ours)	S^2IP-LLM (ICML 2024)	Time-LLM (ICLR 2024)	AutoTimes (NeurIPS 2024)	FPT (NeurIPS 2023)	AMD (AAAI 2025)	ASHyper (NeurIPS 2024)	iTransformer (ICLR 2024)	MSHyper (arXiv 2024)	DLinear (AAAI 2023)	TimesNet (ICLR 2023)	FEDformer (ICML 2022)
Metirc	MSE MAE	MSE MAE	MSE MAE	MSE MAE	MSE MAE	MSE MAE	MSE MAE	MSE MAE	MSE MAE	MSE MAE	MSE MAE	MSE MAE
Weather	**0.217 0.254**	0.223 0.259	0.231 0.269	0.233 0.279	0.237 0.271	0.225 0.265	0.254 0.283	0.305 0.335	0.243 0.271	0.249 0.300	0.259 0.287	0.309 0.360
Electricity	**0.159 0.253**	0.163 0.258	0.165 0.261	0.162 0.261	0.167 0.263	0.162 0.257	0.162 **0.253**	0.203 0.298	0.176 0.276	0.166 0.264	0.193 0.295	0.214 0.327
Traffic	**0.381 0.283**	0.406 0.287	0.408 0.291	0.397 0.289	0.414 0.295	0.412 0.289	0.391 0.289	0.384 0.295	0.393 0.317	0.434 0.295	0.620 0.336	0.610 0.376
ETTh1	**0.402 0.420**	0.405 0.426	0.414 0.435	0.405 0.437	0.418 0.431	0.412 0.428	0.416 0.428	0.451 0.462	0.429 0.437	0.419 0.439	0.520 0.503	0.440 0.460
ETTh2	**0.342 0.383**	0.348 0.392	0.355 0.398	0.358 0.387	0.367 0.402	0.366 0.407	0.351 0.392	0.382 0.414	0.367 0.393	0.502 0.481	0.425 0.451	0.437 0.449
ETTm1	**0.340 0.371**	0.343 0.380	0.350 0.383	0.355 0.380	0.355 0.386	0.352 0.378	0.355 0.381	0.370 0.399	0.388 0.385	0.357 0.380	0.400 0.418	0.448 0.452
ETTm2	**0.252 0.311**	0.257 0.319	0.272 0.332	0.258 0.347	0.264 0.328	0.254 0.315	0.263 0.322	0.272 0.331	0.277 0.326	0.276 0.341	0.305 0.355	0.305 0.349

Results. Table 1 summarizes the results of long-term time series forecasting. We can observe that: (1) MSH-LLM achieves the SOTA results in all datasets. Specifically, MSH-LLM achieves an average error reduction of 4.10% and 3.72% compared to LLM4TS methods (i.e., S^2IP-LLM, AutoTimes, Time-LLM, and FPT), 8.54% and 6.45% compared to latest Transformer-based methods (i.e., ASHyper, iTransformer, and MSHyper), and 7.48% and 5.58% compared to the Linear-based methods (i.e., AMD and DLinear) in MSE and MAE, respectively. (2) By considering group-wise interactions, Ada-MSHyper, MSHyper, and PatchTST achieve competitive performance. (3) Based on this, LLM4TS methods (e.g., S^2IP-LLM and Time-LLM) introduce group-wise interactions into LLMs and generally outperform better than other methods. However, they overlook the multi-scale structures of natural language and time series. (4) By considering the multi-scale structures of natural language and time series, MSH-LLM outperforms other LLM4TS methods in almost all cases.

5.2 SHORT-TERM FORECASTING

Setups. To fully evaluate the performance of MSH-LLM, we also conduct short-term forecasting experiments on M4 datasets, which contain marketing data with different sampling frequencies. More details about M4 dataset are given in Appendix D. The forecasting lengths are set between 6 and 48, which are significantly shorter than those in long-term time series forecasting. Following existing works (Zhou et al., 2023a; Jin et al., 2024; Pan et al., 2024), we set the input length to be twice the forecasting length. The symmetric mean absolute percentage error (SMAPE), mean absolute scaled error (MASE), and overall weighted average (OWA) are used as the evaluation metrics.

Table 2: The average results of short-term time series forecasting on M4 datasets. Lower values mean better performance. The best results are **bolded** and the second best results are underlined. Full results are listed in Appendix G.2, Table 12.

Methods		MSH-LLM (Ours)	AutoTimes (NeurIPS 2024)	S^2IP-LLM (ICML 2024)	Time-LLM (ICLR 2024)	FPT (NeurIPS 2023)	iTransformer (ICLR 2024)	DLinear (AAAI 2023)	PatchTST (ICLR 2023)	N-HiTS (AAAI 2023)	N-BEATS (ICLR 2020)	TimesNet (ICLR 2023)
Avg.	SMAPE	**11.659**	11.831	12.021	12.494	12.690	12.142	13.639	12.059	12.035	12.25	12.88
	MASE	**1.557**	1.585	1.612	1.731	1.808	1.631	2.095	1.623	1.625	1.698	1.836
	OWA	**0.837**	0.850	0.857	0.913	0.940	0.874	1.051	0.869	0.869	0.896	0.955

Results. Table 2 gives the short-term time series forecasting results. We can see that: (1) MSH-LLM performs slightly better than AutoTimes and substantially exceeds other baseline methods. (2) By leveraging LLMs and Patch mechanisms, AutoTimes and PatchTST achieve competitive results than other baseline methods. (3) Compared to AutoTimes and PatchTST, MSH-LLM achieves

superior performance, the reason may be that the hyperedging mechanism can enhance the multi-scale semantic information of time series semantic space while reducing irrelevant information interference.

5.3 Time Series Classification

Setups. We also perform the time series classification task to verify the generalization ability of the model. Following existing works (Zhou et al., 2023a; Wu et al., 2022), we use 10 multivariate UEA time series classification datasets for evaluation, which cover different domains (e.g., gesture, medical diagnosis, and audio recognition). More details about the datasets are given in Appendix G.3. Accuracy is used as the evaluation metric.

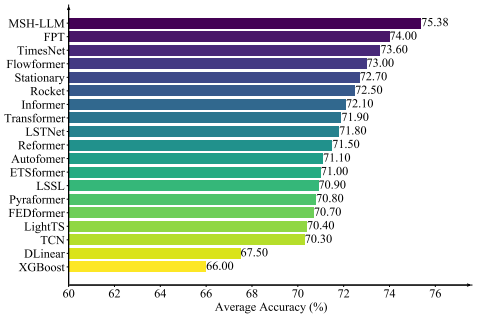

Figure 3: Time series classification results. The results are averaged from 10 subsets of UEA. Higher values mean better performance. Full results are given in Appendix G.3.

Results. Figure 3 shows time series classification results. MSH-LLM achieves an average accuracy of 75.38%, surpassing all baselines including advanced LLM4TS methods FPT (74%). It is also notable that other methods considering multi-scale structures (e.g., TimesNet and Flowformer) can also achieve better performance. The reason is that the time series classification is a sequence-level task, and multi-scale structures help models learn hierarchical representations. However, MSH-LLM still performs better than those methods, the reason may be that MSH-LLM leverages MoP mechanism to enhance the reasoning capabilities of LLMs, thereby promoting LLMs to learn more comprehensive representations of multi-scale temporal patterns.

5.4 Few-Shot Learning

Setups. LLMs have shown impressive capabilities for few-shot learning (Liu et al., 2023a). Following existing works (Jin et al., 2024; Zhou et al., 2023a), we use limited training data (i.e., 5% and 10% of the training data) on 7 commonly used datasets to evaluate the few-short learning performance.

Table 3: Few-shot learning results under 5% training data. Results are averaged from all forecasting lengths. The best results are **bolded** and the second best results are underlined. Full results are listed in Appendix G.4, Table 16.

Methods	MSH-LLM (Ours)	S^2IP-LLM (ICML 2024)	Time-LLM (ICLR 2024)	FPT (NeurIPS 2023)	iTransformer (ICLR 2024)	PatchTST (ICLR 2023)	TimesNet (ICLR 2023)	FEDformer (ICML 2022)	NSFormer (NeurIPS 2022)	ETSformer (arXiv 2022)	Autoformer (NeurIPS 2021)
Metric	MSE MAE	MSE MAE	MSE MAE	MSE MAE	MSE MAE	MSE MAE	MSE MAE	MSE MAE	MSE MAE	MSE MAE	MSE MAE
Weather	**0.247 0.281**	0.260 0.297	0.264 0.301	0.263 0.301	0.309 0.339	0.269 0.303	0.298 0.318	0.309 0.353	0.310 0.353	0.327 0.328	0.333 0.371
Electricity	**0.174 0.269**	0.179 0.275	0.181 0.279	0.178 0.273	0.201 0.296	0.181 0.277	0.402 0.453	0.266 0.353	0.346 0.404	0.627 0.603	0.800 0.685
Traffic	**0.413 0.292**	0.420 0.299	0.423 0.302	0.434 0.305	0.450 0.324	0.418 0.296	0.867 0.493	0.676 0.423	0.833 0.502	1.526 0.839	1.859 0.927
ETT(Avg)	**0.421 0.423**	0.445 0.438	0.580 0.497	0.465 0.447	0.675 0.542	0.590 0.503	0.606 0.507	0.558 0.503	0.587 0.527	0.676 0.526	0.914 0.712

Results. Table 3 summarizes the few-shot learning results under 5% training data. We can see that LLM4TS methods (i.e., MSH-LLM, S^2IP-LLM, and Time-LLM) outperform all other baselines by a large margin. The reason may be that other baseline methods, which are trained from scratch, have limited training data under this scenario. In contrast, LLM4TS methods can apply/align pre-trained knowledge for time series analysis, thereby enhancing its ability to understand and reason time series. Notably, MSH-LLM achieves SOTA results in almost all cases, reducing the prediction error by an average of 10.47% and 6.74% over other LLM4TS methods (i.e., S^2IP-LLM and Time-LLM) in terms of MSE and MAE, respectively. This may attribute to that MSH-LLM can consider the multi-scale structures of natural language and time series, while leveraging the MoP mechanism to unlock the knowledge within LLMs to understand multi-scale patterns. The few-shot learning results under 10% training data are given in Appendix 5.4.

5.5 Zero-Shot Learning

Setups. Except for few-shot learning, LLMs have shown remarkable generalization ability for zero-shot learning. In this section, we evaluate the performance of MSH-LLM for few-shot learning, where no training sample of the target domain is available. Specifically, we adhere to the benchmark established by (Zhou et al., 2023a; Liu et al., 2024) and evaluate the cross-dataset adaptation

performance (i.e., how well the model performance on dataset A when trained on dataset B). M3 and M4 datasets are used to evaluate the zero-shot learning performance.

Table 4: Zero-shot learning results in terms of averaged SMAPE. M4→M3 means training on M4 datasets and testing on M3 datasets, and vice versa. The best results are **bolded** and the second best results are underlined. Full results are listed in Appendix G.5, Table 17.

Methods	MSH-LLM (Ours)	AutoTimes (NeurIPS 2024)	FPT (NeurIPS 2023)	DLinear (AAAI 2023)	PatchTST (ICLR 2023)	TimesNet (ICLR 2023)	NSformer (NeurIPS 2022)	FEDformer (ICML 2022)	Informer (AAAI 2021)	Reformer (ICLR 2019)
M4→M3	**12.469**	12.750	13.060	14.030	13.390	14.170	15.290	13.530	15.820	13.370
M3→M4	**12.968**	13.036	13.125	15.337	13.228	14.553	14.327	15.047	19.047	14.092

Results. Table 4 provides the zero-short learning results. It is notable that both M3 and M4 datasets contain complex multi-scale temporal patterns and show different data distributions. MSH-LLM still achieves the best performance, which may be due to its ability to better leverage the reasoning capabilities of LLMs for interpreting multi-scale temporal patterns. Specifically, MSH-LLM achieves an average of 10.23% SMAPE error reductions across all baselines on average.

5.6 Ablation Studies

LLMs Selection. Scaling law is an essential characteristic that extends from small models to large foundation models. To investigate the impact of backbone model size, we design the following three variants: (1) Using the first 12 Transformer layers of LLaMA-7B (**L.12**). (2) Replacing LLaMA-7B with GPT-2 Small (**G.12**). (3) Replacing LLaMA-7B with the first 6 Transformer layers of GPT-2 Small (**G.6**). The experimental results on Traffic dataset are shown in Table 5. We can observe that MSH-LLM (Default 32) performs better than **L.12**, **G.12**, and **G.6**, which indicate that the scaling law also applies to cross-modalities alignment with frozen LLMs.

Table 5: Results of different LLMs selection and MoP mechanism. The best results are **bolded**.

Methods	**L.12**		**G.12**		**G.6**		-w/o $\mathcal{C}_l$		-w/o $\mathcal{C}_d$		-w/o $\mathcal{C}_c$		-w/o **MoP**		MSH-LLM (**Default**:32)	
Metric	MSE	MAE	MSE	MAE	MSE	MAE	MSE	MAE	MSE	MAE	MSE	MAE	MSE	MAE	MSE	MAE
96	0.370	0.274	0.377	0.281	0.393	0.295	0.373	0.272	0.368	0.273	0.375	0.272	0.399	0.283	**0.365**	**0.270**
192	0.375	0.283	0.385	0.290	0.404	0.297	0.379	0.289	0.383	0.286	0.392	0.282	0.403	0.290	**0.372**	**0.281**
336	0.393	0.286	0.397	0.289	0.411	0.316	0.400	0.293	0.405	0.292	0.391	0.284	0.409	0.295	**0.385**	**0.279**

MoP Mechanism. To investigate the impact of MoP mechanism, we design three variants: (1) Removing the learnable prompts (-w/o $\mathcal{C}_l$). (2) Removing the data-correlated prompts (-w/o $\mathcal{C}_d$). (3) Removing the capability-enhancing prompts (-w/o $\mathcal{C}_c$). (3) Removing the MoP mechanism (-w/o **MoP**). The experimental results on Traffic dataset are shown in Table 5, from which we can observe that MSH-LLM performs better than -w/o $\mathcal{C}_l$, -w/o $\mathcal{C}_d$, and -w/o $\mathcal{C}_c$, showing the effectiveness of learnable prompts, data-correlated prompts, and capability-enhancing prompts, respectively. In addition, -w/o **MoP** achieves the worst performance, demonstrating the effectiveness of the MoP mechanism. More ablation experiments on the MoP mechanism, hyperedging mechanism, ME module, and CMA module are shown in Appendix H and I.

5.7 Parameter Studies

We perform parameter studies on Traffic datasets to evaluate the impact of the max number of hyperedges connected to a node (η) and the number of scales (# scales). The experimental results are shown in Figure 4, from which we can observe that: (1) The best performance can be obtained when $\eta = 4$. The reason is that smaller values of η fail to capture group-wise interactions, while large values of η may introduce noise interference. (2) The optimal # scales is 3. The reason is that smaller # scales limit the expressive ability of MSH-LLM, while large # scales may introduce excessive parameters and cause overfitting problems.

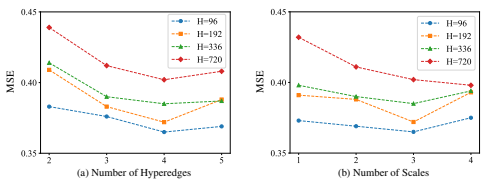

Figure 4: The impact of different hyperparameters.

5.8 Visualization

Visualization of the MoP Mechanism. We perform qualitative analysis to investigate how prompts can guide LLMs in time series analysis. The t-SNE visualization results on Traffic dataset are provided

in Figure 5. We can observe that the output of pre-trained LLMs with the MoP mechanism (Figure 5(a)) shows distinct clusters, while the output of pre-trained LLMs without the MoP mechanism (Figure 5(e)) reveals a more spread-out and lacks clear clustering. The experimental results show the effectiveness of the MoP mechanism in activating the abilities of LLMs to capture multi-scale temporal patterns. In addition, we observe that Figures 5(a) and Figure 5(b) (-w/o $\mathcal{C}_d$) share similar clusters, while Figures 5(c) (-w/o $\mathcal{C}_l$) and Figure 5(d) (-w/o $\mathcal{C}_c$) show less distinct clusters compared to Figure 5(a), suggesting that $\mathcal{C}_d$ has a relatively minor influence compared $\mathcal{C}_l$ and $\mathcal{C}_c$ on Traffic dataset for long-term forecasting. However, this does not imply that $\mathcal{C}_d$ is unimportant, as removing $\mathcal{C}_d$ leads to a performance degradation. The qualitative analysis also aligns with the experimental results in Table 5.

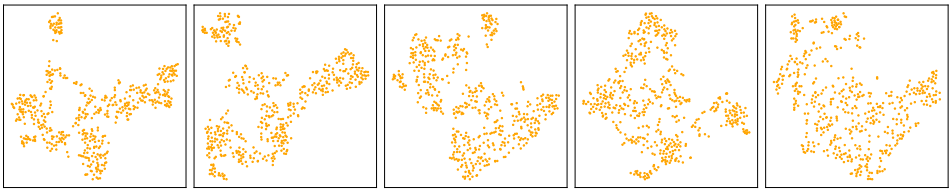

(a) MSH-LLM (b) -w/o $\mathcal{C}_d$ (c) -w/o $\mathcal{C}_c$ (d) -w/o $\mathcal{C}_l$ (e) -w/o MoP

Figure 5: The t-SNE visualization of the output generated by pre-trained LLMs under different prompts.

Visualization of the hyperedge embeddings. We perform qualitative analysis to investigate the training-time trajectories of the hyperedge embeddings. The t-SNE visualization results of hyperedge embeddings on ETTh1 dataset are given in Figure 6. From Figure 6, we can discern the following tendencies: 1) As training progresses, hyperedge embeddings at different scales form distinct clusters. This indicates that MSH-LLM is able to distinguish and capture multi-scale temporal patterns. In addition, even within the same scale, different hyperedge embeddings reside in distinct clusters, indicating the ability of MSH-LLM in capturing diverse temporal patterns within the same scale. 2) From Figure 6(a) to Figure 6(c), we can observe that embeddings of large-scale hyperedges form distinct clusters earlier during training, while embeddings of small-scale hyperedges gradually separate from the large-scale clusters over time. This suggests that during the early stages of training, the model is more focused on capturing coarse-grained temporal patterns (e.g., weekly patterns), and later shifts its focus to learning finer-grained temporal patterns(e.g., hourly and daily patterns).

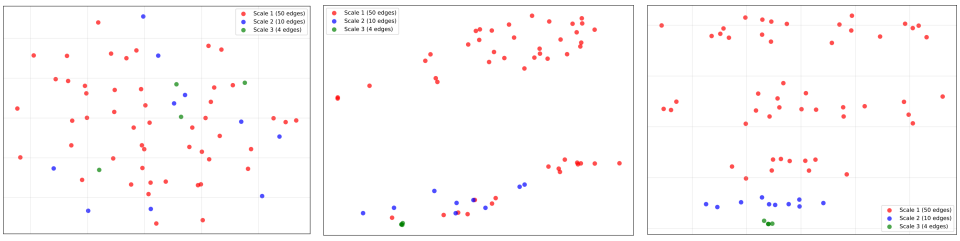

(a) Initial embeddings (b) Embeddings at epoch 1 (c) Embeddings at epoch 3

Figure 6: The t-SNE visualization of hyperedge embeddings at different epochs.

6 Conclusions

In this paper, we propose MSH-LLM, a multi-scale hypergraph framework that aligns pre-trained large language models for time series analysis. Empowered by the hyperedging mechanism and cross-modality alignment (CMA) module, MSH-LLM can perform alignment at different scales, addressing the problem of multi-scale semantic space disparity between natural language and time series. In addition, a mixture of prompts (MoP) mechanism is introduced to enhance the reasoning capabilities of LLMs towards multi-scale temporal patterns. Experimental results on 27 real-world datasets across 5 different applications justify the effectiveness of MSH-LLM.

7 Ethics Statement

Our work focuses solely on scientific problems and does not involve human subjects, animals, or environmentally sensitive materials. We foresee no ethical risks or conflicts of interest.

8 Reproducibility Statement

We have rigorously formalized the model architecture, loss functions, and evaluation metrics through illustrations, equations, and descriptions in the main text. We provide the reproducibility details in the Appendix, including dataset descriptions (Appendix D), experimental details (Appendix E), ablation studies (Appendix H), and visualization (Appendix I). We provide our source code in an anonymous link: https://anonymous.4open.science/r/MSH-LLM-1E9B, which will be publicly available upon acceptance.

References

Ahmed Abdulaal, Zhuanghua Liu, and Tomer Lancewicki. Practical approach to asynchronous multivariate time series anomaly detection and localization. In *Proceedings of the 27th ACM SIGKDD conference on knowledge discovery & data mining*, pp. 2485–2494, 2021.

Josh Achiam, Steven Adler, Sandhini Agarwal, Lama Ahmad, Ilge Akkaya, Florencia Leoni Aleman, Diogo Almeida, Janko Altenschmidt, Sam Altman, Shyamal Anadkat, et al. GPT-4 technical report. *arXiv preprint arXiv:2303.08774*, 2023.

Anthony Bagnall, Hoang Anh Dau, Jason Lines, Michael Flynn, James Large, Aaron Bostrom, Paul Southam, and Eamonn Keogh. The UEA multivariate time series classification archive, 2018. *arXiv preprint arXiv:1811.00075*, 2018.

Song Bai, Feihu Zhang, and Philip HS Torr. Hypergraph convolution and hypergraph attention. *Pattern Recognition*, 110:1–30, 2021.

Hangbo Bao, Li Dong, Songhao Piao, and Furu Wei. BEiT: BERT pre-training of image transformers. In *Proceedings of the International Conference on Learning Representations*, 2022.

Yuxuan Bian, Xuan Ju, Jiangtong Li, Zhijian Xu, Dawei Cheng, and Qiang Xu. Multi-patch prediction: Adapting LLMs for time series representation learning. *arXiv preprint arXiv:2402.04852*, 2024.

Tom B Brown. Language models are few-shot learners. *arXiv preprint arXiv:2005.14165*, 2020.

Defu Cao, Furong Jia, Sercan O Arik, Tomas Pfister, Yixiang Zheng, Wen Ye, and Yan Liu. TEMPO: Prompt-based generative pre-trained transformer for time series forecasting. In *Proceedings of the International Conference on Learning Representations*, 2024.

Cristian Challu, Kin G Olivares, Boris N Oreshkin, Federico Garza Ramirez, Max Mergenthaler Canseco, and Artur Dubrawski. NHiTS: Neural hierarchical interpolation for time series forecasting. In *Proceedings of the AAAI Conference on Artificial Intelligence*, volume 37, pp. 6989–6997, 2023.

Ching Chang, Wen-Chih Peng, and Tien-Fu Chen. LLM4TS: Two-stage fine-tuning for time-series forecasting with pre-trained LLMs. *arXiv preprint arXiv:2308.08469*, 2024.

Donghui Chen, Ling Chen, Zongjiang Shang, Youdong Zhang, Bo Wen, and Chenghu Yang. Scale-aware neural architecture search for multivariate time series forecasting. *ACM Transactions on Knowledge Discovery from Data*, 1:1–22, 2024a.

Junru Chen, Tianyu Cao, Jing Xu, Jiahe Li, Zhilong Chen, Tao Xiao, and Yang Yang. Con4m: Context-aware consistency learning framework for segmented time series classification. *arXiv preprint arXiv:2408.00041*, 2024b.

Peng Chen, Yingying ZHANG, Yunyao Cheng, Yang Shu, Yihang Wang, Qingsong Wen, Bin Yang, and Chenjuan Guo. Pathformer: Multi-scale transformers with adaptive pathways for time series forecasting. In *Proceedings of the International Conference on Learning Representations*, 2023.

Peng Chen, Yingying ZHANG, Yunyao Cheng, Yang Shu, Yihang Wang, Qingsong Wen, Bin Yang, and Chenjuan Guo. Time-MoE: Billion-scale time series foundation models with mixture of experts. In *Proceedings of the International Conference on Learning Representations*, 2025.

Zipeng Chen, Qianli Ma, and Zhenxi Lin. Time-aware multi-scale RNNs for time series modeling. In *Proceedings of the International Joint Conference on Artificial Intelligence*, pp. 2285–2291, 2021.

Jacob Devlin. BERT: Pre-training of deep bidirectional transformers for language understanding. *arXiv preprint arXiv:1810.04805*, 2018.

Hassan Ismail Fawaz, Germain Forestier, Jonathan Weber, Lhassane Idoumghar, and Pierre-Alain Muller. Transfer learning for time series classification. In *IEEE International Conference on Big Data*, pp. 1367–1376, 2018.

Jiaxin Ge, Hongyin Luo, Siyuan Qian, Yulu Gan, Jie Fu, and Shanghang Zhang. Chain of thought prompt tuning in vision language models. *arXiv preprint arXiv:2304.07919*, 2023.

Aaron Grattafiori, Abhimanyu Dubey, Abhinav Jauhri, Abhinav Pandey, Abhishek Kadian, Ahmad Al-Dahle, Aiesha Letman, Akhil Mathur, Alan Schelten, Alex Vaughan, et al. The LLaMA 3 herd of models. *arXiv e-prints arXiv: 2407.21783*, 2024.

Daya Guo, Dejian Yang, Haowei Zhang, Junxiao Song, Ruoyu Zhang, Runxin Xu, Qihao Zhu, Shirong Ma, Peiyi Wang, Xiao Bi, et al. Deepseek-R1: Incentivizing reasoning capability in LLMs via reinforcement learning. *arXiv preprint arXiv:2501.12948*, 2025.

Hansika Hewamalage, Klaus Ackermann, and Christoph Bergmeir. Forecast evaluation for data scientists: Common pitfalls and best practices. *Proceedings of the 29th ACM SIGKDD Conference on Knowledge Discovery & Data Mining*, 37(2):788–832, 2023.

Yifan Hu, Peiyuan Liu, Peng Zhu, Dawei Cheng, and Tao Dai. Adaptive multi-scale decomposition framework for time series forecasting. In *Proceedings of the AAAI Conference on Artificial Intelligence*, volume 39, pp. 17359–17367, 2025.

Yuchi Huang, Qingshan Liu, and Dimitris Metaxas. Video object segmentation by hypergraph cut. In *Proceedings of the IEEE/CVF Conference on Computer Vision and Pattern Recognition*, pp. 1738–1745, 2009.

Kyle Hundman, Valentino Constantinou, Christopher Laporte, Ian Colwell, and Tom Soderstrom. Detecting spacecraft anomalies using lstms and nonparametric dynamic thresholding. In *Proceedings of the 24th ACM SIGKDD international conference on knowledge discovery & data mining*, pp. 387–395, 2018.

Jianwen Jiang, Yuxuan Wei, Yifan Feng, Jingxuan Cao, and Yue Gao. Dynamic hypergraph neural networks. In *Proceedings of the International Joint Conference on Artificial Intelligence*, pp. 2635–2641, 2019.

Ming Jin, Shiyu Wang, Lintao Ma, Zhixuan Chu, James Y Zhang, Xiaoming Shi, Pin-Yu Chen, Yuxuan Liang, Yuan-Fang Li, Shirui Pan, et al. Time-LLM: Time series forecasting by reprogramming large language models. In *Proceedings of the International Conference on Learning Representations*, 2024.

Harshavardhan Kamarthi and B Aditya Prakash. Large pre-trained time series models for cross-domain time series analysis tasks. *arXiv preprint arXiv:2311.11413*, 2023.

Taesung Kim, Jinhee Kim, Yunwon Tae, Cheonbok Park, Jang-Ho Choi, and Jaegul Choo. Reversible instance normalization for accurate time-series forecasting against distribution shift. In *Proceedings of the International Conference on Learning Representations*, 2021.

Diederik P Kingma. Adam: A method for stochastic optimization. *arXiv preprint arXiv:1412.6980*, 2014.

Nikita Kitaev, Lukasz Kaiser, and Anselm Levskaya. Reformer: The efficient transformer. In *Proceedings of the International Conference on Learning Representations*, 2019.

Takeshi Kojima, Shixiang Shane Gu, Machel Reid, Yutaka Matsuo, and Yusuke Iwasawa. Large language models are zero-shot reasoners. *Advances in Neural Information Processing Systems*, 35: 22199–22213, 2022.

Brian Lester, Rami Al-Rfou, and Noah Constant. The power of scale for parameter-efficient prompt tuning. In *Proceedings of the 2021 Conference on Empirical Methods in Natural Language Processing*, pp. 3045–3059, 2021.

Junnan Li, Dongxu Li, Silvio Savarese, and Steven Hoi. Blip-2: Bootstrapping language-image pre-training with frozen image encoders and large language models. In *International conference on machine learning*, pp. 19730–19742. PMLR, 2023.

Chenxi Liu, Qianxiong Xu, Hao Miao, Sun Yang, Lingzheng Zhang, Cheng Long, Ziyue Li, and Rui Zhao. Timecma: Towards llm-empowered multivariate time series forecasting via cross-modality alignment. In *Proceedings of the AAAI Conference on Artificial Intelligence*, volume 39, pp. 18780–18788, 2025a.

Peiyuan Liu, Hang Guo, Tao Dai, Naiqi Li, Jigang Bao, Xudong Ren, Yong Jiang, and Shu-Tao Xia. CALF: Aligning LLMs for time series forecasting via cross-modal fine-tuning. In *Proceedings of the AAAI Conference on Artificial Intelligence*, volume 39, pp. 18915–18923, 2025b.

Shizhan Liu, Hang Yu, Cong Liao, Jianguo Li, Weiyao Lin, Alex X Liu, and Schahram Dustdar. Pyraformer: Low-complexity pyramidal attention for long-range time series modeling and forecasting. In *Proceedings of the International Conference on Learning Representations*, 2021.

Xin Liu, Daniel McDuff, Geza Kovacs, Isaac Galatzer-Levy, Jacob Sunshine, Jiening Zhan, Ming-Zher Poh, Shun Liao, Paolo Di Achille, and Shwetak Patel. Large language models are few-shot health learners. *arXiv preprint arXiv:2305.15525*, 2023a.

Yong Liu, Haixu Wu, Jianmin Wang, and Mingsheng Long. Non-stationary transformers: Exploring the stationarity in time series forecasting. *Advances in Neural Information Processing Systems*, 35: 9881–9893, 2022.

Yong Liu, Tengge Hu, Haoran Zhang, Haixu Wu, Shiyu Wang, Lintao Ma, and Mingsheng Long. iTransformer: Inverted transformers are effective for time series forecasting. In *Proceedings of the International Conference on Learning Representations*, 2023b.

Yong Liu, Guo Qin, Xiangdong Huang, Jianmin Wang, and Mingsheng Long. Autotimes: Autoregressive time series forecasters via large language models. *Advances in Neural Information Processing Systems*, 37:122154–122184, 2024.

Aditya P Mathur and Nils Ole Tippenhauer. Swat: A water treatment testbed for research and training on ics security. In *2016 international workshop on cyber-physical systems for smart water networks (CySWater)*, pp. 31–36. IEEE, 2016.

Yuqi Nie, Nam H Nguyen, Phanwadee Sinthong, and Jayant Kalagnanam. A time series is worth 64 words: Long-term forecasting with transformers. In *Proceedings of the International Conference on Learning Representations*, 2022.

Boris N Oreshkin, Dmitri Carpov, Nicolas Chapados, and Yoshua Bengio. N-BEATS: Neural basis expansion analysis for interpretable time series forecasting. In *Proceedings of the International Conference on Learning Representations*, 2020.

Zijie Pan, Yushan Jiang, Sahil Garg, Anderson Schneider, Yuriy Nevmyvaka, and Dongjin Song. S^2IP-LLM: Semantic space informed prompt learning with LLM for time series forecasting. In *Proceedings of the International Conference on Machine Learning*, pp. 39135–39153, 2024.

Adam Paszke, Sam Gross, Francisco Massa, Adam Lerer, James Bradbury, Gregory Chanan, Trevor Killeen, Zeming Lin, Natalia Gimelshein, Luca Antiga, et al. Pytorch: An imperative style, high-performance deep learning library. *Advances in Neural Information Processing Systems*, 32: 1–12, 2019.

Renjie Pi, Lewei Yao, Jiahui Gao, Jipeng Zhang, and Tong Zhang. PerceptionGPT: Effectively fusing visual perception into LLM. In *Proceedings of the IEEE/CVF Conference on Computer Vision and Pattern Recognition*, pp. 27124–27133, 2024.

Alec Radford, Jeffrey Wu, Rewon Child, David Luan, Dario Amodei, Ilya Sutskever, et al. Language models are unsupervised multitask learners. *OpenAI blog*, 1(8):9, 2019.

Alec Radford, Jong Wook Kim, Chris Hallacy, Aditya Ramesh, Gabriel Goh, Sandhini Agarwal, Girish Sastry, Amanda Askell, Pamela Mishkin, Jack Clark, et al. Learning transferable visual models from natural language supervision. In *Proceedings of the International Conference on Machine Learning*, pp. 8748–8763, 2021.

Ramit Sawhney, Shivam Agarwal, Arnav Wadhwa, Tyler Derr, and Rajiv Ratn Shah. Stock selection via spatiotemporal hypergraph attention network: A learning to rank approach. In *Proceedings of the AAAI Conference on Artificial Intelligence*, volume 35, pp. 497–504, 2021.

Zongjiang Shang, Ling Chen, Binqing Wu, and Dongliang Cui. Ada-MSHyper: Adaptive multi-scale hypergraph transformer for time series forecasting. *Advances in Neural Information Processing Systems*, 37:33310–33337, 2024a.

Zongjiang Shang, Ling Chen, Binqing Wu, and Liangcui Dong. MSHyper: Multi-scale hypergraph transformer for long-range time series forecasting. *arXiv preprint arXiv:2401.09261*, 2024b.

Ya Su, Youjian Zhao, Chenhao Niu, Rong Liu, Wei Sun, and Dan Pei. Robust anomaly detection for multivariate time series through stochastic recurrent neural network. In *Proceedings of the 25th ACM SIGKDD international conference on knowledge discovery & data mining*, pp. 2828–2837, 2019.

Chenxi Sun, Hongyan Li, Yaliang Li, and Shenda Hong. TEST: Text prototype aligned embedding to activate LLM's ability for time series. In *Proceedings of the International Conference on Learning Representations*, 2024.

Mingtian Tan, Mike Merrill, Vinayak Gupta, Tim Althoff, and Tom Hartvigsen. Are language models actually useful for time series forecasting? *Advances in Neural Information Processing Systems*, 37:60162–60191, 2024.

Xing Tang, Ling Chen, Hongyu Shi, and Dandan Lyu. DHyper: A recurrent dual hypergraph neural network for event prediction in temporal knowledge graphs. *ACM Transactions on Information Systems*, 2024.

Changyuan Tian, Zhicong Lu, Zequn Zhang, Heming Yang, Wei Cao, Zhi Guo, Xian Sun, and Li Jin. HyperMixer: Specializable hypergraph channel mixing for long-term multivariate time series forecasting. In *Proceedings of the AAAI Conference on Artificial Intelligence*, volume 39, pp. 20885–20893, 2025.

Hugo Touvron, Matthieu Cord, Matthijs Douze, Francisco Massa, Alexandre Sablayrolles, and Hervé Jégou. Training data-efficient image transformers & distillation through attention. In *Proceedings of the International Conference on Machine Learning*, pp. 10347–10357, 2021.

Hugo Touvron, Thibaut Lavril, Gautier Izacard, Xavier Martinet, Marie-Anne Lachaux, Timothée Lacroix, Baptiste Rozière, Naman Goyal, Eric Hambro, Faisal Azhar, et al. LLaMA: Open and efficient foundation language models. *arXiv preprint arXiv:2302.13971*, 2023.

Guancheng Wan, Zewen Liu, Max SY Lau, B Aditya Prakash, and Wei Jin. Epidemiology-aware neural ode with continuous disease transmission graph. *arXiv preprint arXiv:2410.00049*, 2024.

Jun Wang, Wenjie Du, Wei Cao, Keli Zhang, Wenjia Wang, Yuxuan Liang, and Qingsong Wen. Deep learning for multivariate time series imputation: A survey. *arXiv preprint arXiv:2402.04059*, 2024a.

Pichao Wang, Xue Wang, Fan Wang, Ming Lin, Shuning Chang, Hao Li, and Rong Jin. Kvt: k-nn attention for boosting vision transformers. In *European conference on computer vision*, pp. 285–302. Springer, 2022.

Wenhai Wang, Jifeng Dai, Zhe Chen, Zhenhang Huang, Zhiqi Li, Xizhou Zhu, Xiaowei Hu, Tong Lu, Lewei Lu, Hongsheng Li, et al. Internimage: Exploring large-scale vision foundation models with deformable convolutions. In *Proceedings of the IEEE/CVF Conference on Computer Vision and Pattern Recognition*, pp. 14408–14419, 2023.

Wenhai Wang, Zhe Chen, Xiaokang Chen, Jiannan Wu, Xizhou Zhu, Gang Zeng, Ping Luo, Tong Lu, Jie Zhou, Yu Qiao, et al. VisionLLM: Large language model is also an open-ended decoder for vision-centric tasks. *Advances in Neural Information Processing Systems*, 36:61501–61513, 2024b.

Yihe Wang, Nan Huang, Taida Li, Yujun Yan, and Xiang Zhang. Medformer: A multi-granularity patching transformer for medical time-series classification. *arXiv preprint arXiv:2405.19363*, 2024c.

Qingsong Wen, Kai He, Liang Sun, Yingying Zhang, Min Ke, and Huan Xu. RobustPeriod: Robust time-frequency mining for multiple periodicity detection. In *Proceedings of the International Monference on Management of Data*, pp. 2328–2337, 2021.

Gerald Woo, Chenghao Liu, Doyen Sahoo, Akshat Kumar, and Steven Hoi. CoST: Contrastive learning of disentangled seasonal-trend representations for time series forecasting. In *Proceedings of the International Conference on Learning Representations*, 2022a.

Gerald Woo, Chenghao Liu, Doyen Sahoo, Akshat Kumar, and Steven Hoi. ETSformer: Exponential smoothing transformers for time-series forecasting. *arXiv preprint arXiv:2202.01381*, 2022b.

Haixu Wu, Jiehui Xu, Jianmin Wang, and Mingsheng Long. Autoformer: Decomposition transformers with auto-correlation for long-term series forecasting. *Advances in Neural Information Processing Systems*, pp. 22419–22430, 2021.

Haixu Wu, Tengge Hu, Yong Liu, Hang Zhou, Jianmin Wang, and Mingsheng Long. TimesNet: Temporal 2d-variation modeling for general time series analysis. In *Proceedings of the International Conference on Learning Representations*, 2022.

Chenxin Xu, Maosen Li, Zhenyang Ni, Ya Zhang, and Siheng Chen. GroupNet: Multiscale hypergraph neural networks for trajectory prediction with relational reasoning. In *Proceedings of the IEEE/CVF Conference on Computer Vision and Pattern Recognition*, pp. 6498–6507, 2022.

Hao Xue and Flora D Salim. Promptcast: A new prompt-based learning paradigm for time series forecasting. *IEEE Transactions on Knowledge and Data Engineering*, 36(11):6851–6864, 2023.

Naganand Yadati, Madhav Nimishakavi, Prateek Yadav, Vikram Nitin, Anand Louis, and Partha Talukdar. HyperGCN: A new method for training graph convolutional networks on hypergraphs. *Advances in Neural Information Processing Systems*, 32:1511–1522, 2019.

An Yang, Baosong Yang, Beichen Zhang, Binyuan Hui, Bo Zheng, Bowen Yu, Chengyuan Li, Dayiheng Liu, Fei Huang, Haoran Wei, et al. Qwen2. 5 technical report. *arXiv preprint arXiv:2412.15115*, 2024a.

Rui Yang, Shuang Wang, Yingping Han, Yuanheng Li, Dong Zhao, Dou Quan, Yanhe Guo, Licheng Jiao, and Zhi Yang. Transcending fusion: A multi-scale alignment method for remote sensing image-text retrieval. *IEEE Transactions on Geoscience and Remote Sensing*, 2024b.

Ailing Zeng, Muxi Chen, Lei Zhang, and Qiang Xu. Are transformers effective for time series forecasting? *arXiv preprint arXiv:2205.13504*, 2022.

George Zerveas, Srideepika Jayaraman, Dhaval Patel, Anuradha Bhamidipaty, and Carsten Eickhoff. A transformer-based framework for multivariate time series representation learning. In *Proceedings of the 27th ACM SIGKDD Conference on Knowledge Discovery & Data Mining*, pp. 2114–2124, 2021.

Yusheng Zhao, Xiao Luo, Wei Ju, Chong Chen, Xian-Sheng Hua, and Ming Zhang. Dynamic hypergraph structure learning for traffic flow forecasting. In *IEEE International Conference on Data Engineering*, pp. 2303–2316, 2023.

Haoyi Zhou, Shanghang Zhang, Jieqi Peng, Shuai Zhang, Jianxin Li, Hui Xiong, and Wancai Zhang. Informer: Beyond efficient transformer for long sequence time-series forecasting. In *Proceedings of the AAAI Conference on Artificial Intelligence*, volume 35, pp. 11106–11115, 2021.

Tian Zhou, Ziqing Ma, Qingsong Wen, Xue Wang, Liang Sun, and Rong Jin. FEDformer: Frequency enhanced decomposed transformer for long-term series forecasting. In *Proceedings of the International Conference on Machine Learning*, pp. 27268–27286, 2022.

Tian Zhou, Peisong Niu, Liang Sun, Rong Jin, et al. One fits all: Power general time series analysis by pretrained LM. *Advances in Neural Information Processing Systems*, 36:43322–43355, 2023a.

Yongchao Zhou, Andrei Ioan Muresanu, Ziwen Han, Keiran Paster, Silviu Pitis, Harris Chan, and Jimmy Ba. Large language models are human-level prompt engineers. In *Proceedings of the International Conference on Learning Representations*, 2023b.

A DESCRIPTION OF NOTATIONS

To help understand the symbols used throughout the paper, we provide a detailed list of the key notations in Table 6.

Table 6: Description of the key notations.

Notation	Descriptions
$\mathcal{G}$	Hypergraph
$\mathcal{E}$	Hyperedge set
$\mathcal{V}$	Node set
N^s	Number of nodes at scale s
M^s	Number of hyperedges at scale s
T	Input length
H	Output length
D	Temporal feature dimension
s	Scale index
S	Number of temporal scales
$\mathbf{X}^{\mathrm{I}}_{1:T}$	Input time series
$\mathbf{X}^s$	Sub-sequence at scale s
θ^{s-1}	Learnable parameters of the aggregation function at scale $s-1$
$\boldsymbol{x}_t$	Values at time step t
$\mathbf{U}$	Word token embeddings of pre-trained LLMs
V	Vocabulary size
P	Hidden dimension size of LLMs
$\mathbf{U}^s$	Prototypes at scale s
λ^{s-1}	Learnable parameters of the linear mapping function at scale $s-1$
$\boldsymbol{E}^s_{\mathrm{node}} \in \mathbb{R}^{N^s \times D}$	Node embeddings at scale s
$\boldsymbol{E}^s_{\mathrm{hyper}} \in \mathbb{R}^{M^s \times D}$	Hyperedge embeddings at scale s
e^s_i	ith hyperedge at scale s
x^s_i	ith node at scale s
$\boldsymbol{e}^s_i$	ith hyperedge feature representation at scale s
$\boldsymbol{x}^s_i$	ith node feature representation at scale s
η	Threshold of $TopK$ function
$\boldsymbol{\mathcal{E}}^s$	Hyperedge feature set at scale s
$\mathbf{H}^s$	Incidence matrix at scale s
$\boldsymbol{\beta} \in \mathbb{R}^{1\times 1}$	Learnable parameters
$\boldsymbol{\varphi} \in \mathbb{R}^{1\times 1}$	Learnable parameters
l^{s-1}	Size of the aggregation window at scale $s-1$
$\mathcal{N}(e^s_i)$	Nodes connected by e^s_i
$\mathbf{Q}^s_\jmath, \mathbf{K}^s_\jmath, \mathbf{V}^s_\jmath$	Queries, keys, and values of the $\jmath$ head at scale s
$\jmath$	Head index
$\mathcal{J}$	Number of heads
$\boldsymbol{\mathcal{Z}}^s$	Cross-modality aligned features
$\boldsymbol{\mathcal{C}}_l$	Learnable prompts
$\mathbf{P}^s$	Scale-specific prompts
L^s	Length of learnable prompts at scale s
$\boldsymbol{\mathcal{C}}_d$	Data-correlated prompts
π, τ, μ	Dataset description, task introduction, and dataset statistics prompts
ϕ, φ, ψ	Logical thinking, emotional manipulation, and time series reasoning prompts
$\boldsymbol{\mathcal{C}}_c$	Capability-enhancing prompts
$[.,.]$	Concatenation operation
$\mathcal{O}$	Output representation

B DESCRIPTION OF BASELINES

We compare MSH-LLM with 19 competitive baselines. Below are brief descriptions of the baselines:

AutoTimes (Liu et al., 2024): AutoTimes repurposes frozen LLMs as autoregressive time series forecasters and introduces time series-related prompts to enhance forecasting.

Time-LLM (Jin et al., 2024): Time-LLM introduces a patch reprogramming mechanism to align the input time series with text prototypes, and then feeds the aligned features into frozen LLMs to get the output results.

FPT (Zhou et al., 2023a): FPT fine-tunes the key parameters of LLMs and transforms the LLMs into a unified framework for time series analysis.

S^2IP-LLM (Pan et al., 2024): S^2IP-LLM aligns the semantic space of LLMs with that of time series and performs time series forecasting based on learned prompts from the joint space.

DLinear (Zeng et al., 2022): DLinear decomposes the input time series into seasonal and trend components, and employs a linear layer for each component to model temporal dependencies.

N-HiTS (Challu et al., 2023): N-HiTS proposes a novel hierarchical interpolation and multi-rate data sampling techniques to model multi-scale temporal patterns.

N-BEATS (Oreshkin et al., 2020): N-BEATS employs a deep stack of fully-connected layers based on backward and forward residual connections to model temporal dependencies.

AMD (Hu et al., 2025): AMD decomposes time series into distinct temporal patterns at different scales and leverages the multi-scale decomposable mixing block to dissect and aggregate these patterns in a residual manner.

Ada-MSHyper (Shang et al., 2024a): Ada-MSHyper utilizes an adaptive hypergraph to capture group-wise interactions at different scales and introduces a constraint mechanism to address the problem of temporal variations entanglement.

iTransformer (Liu et al., 2023b): iTransformer embeds individual time points of time series into variate tokens, then applies the attention mechanism and feed-forward network to capture variate correlations and learn nonlinear representations, respectively.

PatchTST (Nie et al., 2022): PatchTST segments time series into subsequence-level patches and treats them as input tokens to model temporal dependencies in a channel-independent manner.

TimesNet (Wu et al., 2022): TimesNet transforms 1D time series into a set of 2D tensors by multi-periodicity analysis to model complex temporal variations from a 2D perspective.

MSHyper (Shang et al., 2024b): MSHyper constructs multi-scale hypergraphs in a rule-based manner and combines them with a tri-stage message passing mechanism to model group-wise interactions between multi-scale temporal patterns.

Autoformer (Wu et al., 2021): Autoformer utilizes a decomposition architecture with an auto-correlation mechanism to discover the long-range dependencies.

NSFormer (Liu et al., 2022): NSFormer introduces a series stationarization module and a de-stationary attention module to improve the predictability of time series and address the over-stationarization problem, respectively.

FEDformer (Zhou et al., 2022): FEDformer utilizes a decomposition method to capture the global information of time series and a frequency-enhanced block to capture important structures.

ETSformer (Woo et al., 2022b): ETSformer incorporates the principles of exponential smoothing by replacing traditional self-attention with exponential smoothing attention and frequency attention for time series forecasting.

Reformer (Kitaev et al., 2019): Reformer approximates the attention value through local-sensitive hashing (LSH) and leverages reversible residual layers to reduce the computation cost.

Informer (Zhou et al., 2021): Informer selects dominant query by calculating KL-divergence to reduce computational complexity and utilizes a generative style decoder to accelerate inference speed.

C Description of Hypergraph Learning

Compared to Graph Neural Networks (GNNs), which model pairwise interactions by operating on graphs where each edge connects exactly two nodes, Hypergraph Neural Networks (HGNNs) generalize this paradigm to capture group-wise interactions through hyperedges that can connect an arbitrary number of nodes. As shown in Figure 7, the graph is represented using the adjacency matrix, in which each edge connects two nodes. In contrast, the hypergraph is represented by the incidence matrix, which can capture group-wise interaction using its degree-free hyperedges.

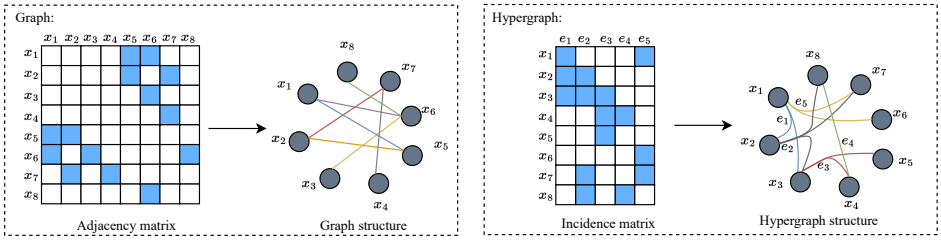

Figure 7: The comparison between graph and hypergraph.

Recently, HGNNs have been applied in different fields, e.g., video object segmentation (Huang et al., 2009), stock selection (Sawhney et al., 2021), temporal knowledge graphs (Tang et al., 2024), and time series forecasting (Shang et al., 2024a;b; Zhao et al., 2023; Tian et al., 2025). HyperGCN (Yadati et al., 2019) is the first work to incorporate convolutional operations into hypergraphs, demonstrating the superiority of HGNNs over ordinary GNNs in capturing group-wise interactions. STHAN-SR (Sawhney et al., 2021) reformulates stock prediction as a learning-to-rank task and utilizes hypergraphs to capture group-wise interactions between stocks. GroupNet (Xu et al., 2022) employs multi-scale hypergraphs for trajectory prediction, which combines relational reasoning with hypergraph structures to capture group-wise pattern interactions among multiple agents. In the context of time series forecasting, MSHyper (Shang et al., 2024b) is the first work to incorporate hypergraphs into long-term time series forecasting, which leverages predefined hypergraphs and the tri-stage message passing mechanism to capture multi-scale pattern interactions. Building on this, Ada-MSHyper (Shang et al., 2024a) introduces adaptive hypergraph modeling, which combines adaptive hypergraphs with the node and hyperedge constraint mechanism to capture abundant and implicit group-wise temporal pattern interactions.

In this paper, we represent temporal features of different scales as nodes and use learnable hyperedges in the hypergraph to capture group-wise interactions, thereby enhancing the semantic information of time series semantic space. We formulate this process as the hyperedging mechanism. As mentioned above, our hyperedging mechanism differs from previous methods in two aspects. Firstly, our methods can capture implicit group-wise interactions at different scales in a learnable manner, while most existing methods (Nie et al., 2022; Zhou et al., 2023a; Shang et al., 2024b) rely on pre-defined rules to model group-wise interactions at a single scale. Secondly, although some methods (Shang et al., 2024a; Jiang et al., 2019) learn from hypergraphs, they focus on constraints or clustering-based approaches to learn the hypergraph structures. In contrast, our method learns the hypergraph structures in a pure data-driven manner by incorporating learnable parameters and nonlinear transformations, which is more flexible and can learn more complex hypergraph structures.

D Description of Datasets

Datasets for Long-Term Forecasting and Few-Shot Learning. For long-term time series forecasting and few-shot learning, we conduct experiments on 7 commonly used datasets, including Electricity Transformers Temperature (ETT), Traffic[1], Electricity[2], and Weather[3] datasets following existing works (Zhou et al., 2023a; Pan et al., 2024; Jin et al., 2024). ETT datasets include data from two counties in China. The datasets are further divided into four subsets with different sampling

[1] http://pems.dot.ca.gov

[2] https://archive.ics.uci.edu/ml/datasets/ElectricityLoadDiagrams20112014

[3] https://www.bgc-jena.mpg.de/wetter/

frequencies: ETTm1 and ETTm2, which are sampled every 15 minutes, and ETTh1 and ETTh2, which are sampled hourly. Each subset contains seven variables, including the target variable 'oil temperature' and six power load variables. Traffic dataset provides hourly road occupancy rates, which are sampled from 821 freeway sensors across the state of California. Electricity dataset comprises hourly electricity consumption data of 321 clients. Weather dataset records 21 meteorological indicators collected every 10 minutes from weather stations in Germany. The detailed descriptions of the datasets are given in Table 7.

Table 7: Dataset descriptions for long-term time series forecasting and few-shot learning.

Dataset	Variates	Forecasting Length	Frequency	Information
ETTh1, ETTh2	7	(96, 192, 336, 720)	Hourly	Temperature
ETTm1, ETTm2	7	(96, 192, 336, 720)	15 mins	Temperature
Electricity	321	(96, 192, 336, 720)	Hourly	Electricity
Traffic	862	(96, 192, 336, 720)	Hourly	Transportation
Weather	21	(96, 192, 336, 720)	10 mins	Weather

We follow the same data processing and training-validation-testing split protocol as in existing works (Zhou et al., 2023a; Jin et al., 2024; Pan et al., 2024). Each dataset is split into training, validation, and testing sets based on chronological order. For ETT datasets (i.e., ETTh1, ETTh2, ETTm1, and ETTm2), the split ratio of training-validation-testing sets is 6:2:2. For Traffic, Electricity, and Weather datasets, the split ratio is 7:2:1. For the few-shot learning task, only a portion (5% or 10%) of training data is used, while the validation and testing sets remain unchanged.

Datasets for Short-Term Forecasting and Zero-Shot Learning. Following existing works (Liu et al., 2024; Zhou et al., 2023a), we leverage M4 dataset for short-term forecasting and use both M3 and M4 datasets for zero-shot learning. M4 dataset is a large dataset that covers different domains (e.g., demographic, financial, and industry) and has been divided into six subsets based on different sampling frequencies that range from hourly to yearly. M3 dataset is smaller than M4 but also contains time series with different sampling frequencies. The detailed descriptions of M3 and M4 datasets are outlined in Table 8.

Table 8: Dataset descriptions for short-term time series forecasting and zero-shot learning. The dataset size is organized in (training, validation, and testing).

Dataset	Forecasting Length	Dataset Size	Frequency	Information	Mapping
M3 Yearly	6	(645, 0, 645)	Yearly	Demographic	M4 Yearly
M3 Quarterly	8	(756, 0, 756)	Quarterly	Finance	M4 Quarterly
M3 Monthly	18	(1428, 0, 1428)	Monthly	Industry	M4 Monthly
M3 Others	8	(174, 0, 174)	Weekly	Macro	M4 Quarterly
M4 Yearly	6	(23000, 0, 23000)	Yearly	Demographic	M3 Yearly
M4 Quarterly	8	(24000, 0, 24000)	Quarterly	Finance	M3 Quarterly
M4 Monthly	18	(48000, 0, 48000)	Monthly	Industry	M3 Monthly
M4 Weekly	13	(359, 0, 359)	Weekly	Macro	M3 Monthly
M4 Daily	14	(4227, 0, 4227)	Daily	Micro	M3 Monthly
M4 Hourly	48	(414, 0, 414)	Hourly	Other	M3 Monthly

Datasets for Time Series Classification. Following existing works (Zhou et al., 2023a; Wu et al., 2022), we use 10 multivariate datasets selected from the UEA time series classification Archive (Bagnall et al., 2018; Zerveas et al., 2021) for time series classification. These datasets are complex, which cover different domains (e.g., gesture, medical diagnosis, and audio recognition) and exhibit diverse characteristics in terms of sample size, dimensionality, and number of classes. The detailed descriptions of the datasets are provided in Table 9.

E Experimental Settings

MSH-LLM is implemented in PyTorch (Paszke et al., 2019), with all experiments conducted on NVIDIA A100-80 GPUs and NVIDIA GeForce RTX 3090 GPUs. We use LLaMA-7B (Touvron et al., 2023) as the default base LLM unless specified otherwise. We repeat all experiments 3 times and use the mean as the final results. Adam (Kingma, 2014) is used as the optimizer with the initial

Table 9: Dataset descriptions for time series classification. The dataset size is organized in (training, validation, and testing).

Dataset	Dataset size	Variates	Classes	Information
EthanolConcentration	(261, 0, 263)	3	4	Biomedical
FaceDetection	(5890, 0, 3524)	144	2	Computer Vision
Handwriting	(150, 0, 850)	3	26	Pattern Recognition
Heartbeat	(204, 0, 205)	61	2	Medical Recognition
JapaneseVowels	(270, 0, 370)	12	9	Audio Recognition
PEMS-SF	(267, 0, 173)	963	7	Transportation
SelfRegulationSCP1	(268, 0, 293)	6	2	Psychology
SelfRegulationSCP2	(200, 0, 180)	7	2	Psychology
SpokenArabicDigits	(6599, 0, 2199)	13	10	Speech Recognition
UWaveGestureLibrary	(120, 0, 320)	3	8	Gesture

learning rate chosen from $\{10^{-3}, 5 \times 10^{-3}, 10^{-4}\}$. The total number of scales S is set to 3. We use 1D convolution as our aggregation function. For other key hyperparameters, unlike existing works that use grid search over tunable hyperparameters, we leverage Neural Network Intelligence (NNI) [4] toolkit to automatically search for the best hyperparameters. The detailed search space of key hyperparameters is given in Table 10. Following existing works (Zhou et al., 2023a; Wu et al., 2022), we adopt MSE as the objective function for long-term time series forecasting and few-shot learning tasks. For short-term time series forecasting and zero-shot learning, we use SMAPE as the objective function. It is notable that some baselines cannot be used directly due to different choices of input and output lengths. For a fair comparison, we primarily adopt the results from existing papers (Jin et al., 2024; Zhou et al., 2023a; Pan et al., 2024). For other results, we utilize their official code while adjusting the input and out lengths. The source code of MSH-LLM is released on Anonymous GitHub [5].

Table 10: The search space of hyperparameters.

Parameters	Choise
Batch size	{8, 16, 32, 64, 128, 256}
Number of hyperedges at scale 1	{5, 10, 20, 30, 50}
Number of hyperedges at scale 2	{2, 5, 10, 15, 20}
Number of hyperedges at scale 3	{1, 2, 4, 5, 8, 12}
Number of text prototypes at scale 1	{20, 50, 100, 200, 500, 1000}
Number of text prototypes at scale 1	{10, 25, 50, 100, 200, 500}
Number of text prototypes at scale 1	{4, 5, 10, 25, 50, 100}
Aggregation window size at scale 1	{2, 4, 8}
Aggregation window size at scale 2	{2, 4}
η	{2, 3, 4, 5, 10, 15, 20}

F Evaluation Metrics

For long-term time series forecasting and few-shot learning, we employ the Mean Squared Error (MSE) and Mean Absolute Error (MAE) as our evaluation metrics, which can be formulated as follows:

$$\text{MSE} = \frac{1}{H}\left\|\widehat{\mathbf{X}}^{\text{O}}_{T+1:T+H} - \mathbf{X}^{\text{O}}_{T+1:T+H}\right\|_2^2, \quad \text{MAE} = \frac{1}{H}\left|\widehat{\mathbf{X}}^{\text{O}}_{T+1:T+H} - \mathbf{X}^{\text{O}}_{T+1:T+H}\right|, \tag{10}$$

where T and H are the input and output lengths, $\widehat{\mathbf{X}}^{\text{O}}_{T+1:T+H}$ and $\mathbf{X}^{\text{O}}_{T+1:T+H}$ are the forecasting results and ground truth, respectively.

For short-term time series forecasting and zero-shot learning on M4 benchmark, we adopt the Symmetric Mean Absolute Percentage Error (SMAPE), Mean Absolute Scaled Error (MASE), and

[4] https://nni.readthedocs.io/en/latest/

[5] https://anonymous.4open.science/r/MSH-LLM-1E9B

Overall Weighted Average (OWA) as our evaluation metrics, which can be formulated as follows:

$$\text{SMAPE} = \frac{200}{H}\sum_{h=1}^{H}\frac{|\widehat{\mathbf{X}}^{\text{O}}_{T+1:T+H} - \mathbf{X}^{\text{O}}_{T+1:T+H}|}{|\mathbf{X}^{\text{O}}_{T+1:T+H}|}, \tag{11}$$

$$\text{MASE} = \frac{1}{H}\sum_{h=1}^{H}\frac{|\widehat{\mathbf{X}}^{\text{O}}_{T+1:T+H} - \mathbf{X}^{\text{O}}_{T+1:T+H}|}{\frac{1}{H-s}\sum_{j=s+1}^{H}|\mathbf{X}^{\text{O}}_{T+1:T+H} - \mathbf{X}^{\text{O}}_{T+1:T+H-1}|}, \tag{12}$$

$$\text{OWA} = \frac{1}{2}\left[\frac{\text{SMAPE}}{\text{SMAPE}_{\text{Naive2}}} + \frac{\text{MASE}}{\text{MASE}_{\text{Naive2}}}\right], \tag{13}$$

Notably, the OWA metric is a specific metric that is only used for short-term time series forecasting.

G Full Results

We compare MSH-LLM with 19 baselines that cover five different applications: Long-term time series forecasting, short-term time series forecasting, time series classification, few-shot learning, and zero-shot learning. For a fair comparison, we follow the unified experimental settings used in existing works (Zhou et al., 2023a; Pan et al., 2024; Jin et al., 2024). The average results refer to the mean of results under different forecasting results, where the best results are **bolded** and the second best results are underlined. * indicates that some results do not meet the unified settings, thus we rerun their official code under unified settings and fine-tune their key hyperparameters.

G.1 Long-Term Time Series Forecasting

Table 11 summarizes the full results of long-term time series forecasting. We can observe that MSH-LLM achieves the SOTA results in 54 out of 70 cases across 7 time series datasets. Specifically, on the well-studied Traffic datast, MSH-LLM achieves an average error reduction of 11.54% and 6.71% across all baselines. On the challenging Weather dataset, MSH-LLM achieves an average error reduction of 12.78% and 11.26% across all baselines.

Table 11: Full results of long-term time series forecasting. The input length is set to 512, and the forecasting lengths are set to 96, 192, 336, and 720. Lower values mean better performance. The best results are **bolded** and the second best results are underlined.

Methods		MSH-LLM (Ours)		S^2IP-LLM (ICLR 2024)		Time-LLM (ICLR 2024)		AutoTimes* (NeurIPS 2024)		FPT (NeurIPS 2023)		AMD* (AAAI 2025)		ASHyper* (NeurIPS 2024)		iTransformer (ICLR 2024)		MSHyper* (arXiv 2024)		DLinear (AAAI 2023)		TimesNet (ICLR 2023)		FEDformer (ICML 2022)	
Metric		MSE	MAE	MSE	MAE	MSE	MAE	MSE	MAE	MSE	MAE	MSE	MAE	MSE	MAE	MSE	MAE	MSE	MAE	MSE	MAE	MSE	MAE	MSE	MAE
Weather	96	**0.138**	**0.187**	0.145	0.195	0.158	0.210	0.161	0.216	0.162	0.212	0.148	0.203	0.169	0.228	0.253	0.304	0.171	0.212	0.176	0.237	0.172	0.220	0.217	0.296
	192	**0.187**	**0.230**	0.190	0.235	0.197	0.245	0.205	0.253	0.204	0.248	0.193	0.243	0.235	0.288	0.280	0.319	0.214	0.250	0.220	0.282	0.219	0.261	0.276	0.336
	336	**0.237**	0.282	0.243	**0.280**	0.248	0.285	0.251	0.289	0.254	0.286	0.242	0.281	0.275	0.287	0.321	0.344	0.260	0.287	0.265	0.319	0.280	0.306	0.339	0.380
	720	**0.305**	**0.315**	0.312	0.326	0.319	0.334	0.314	0.356	0.326	0.337	0.315	0.332	0.335	0.327	0.364	0.374	0.327	0.336	0.333	0.362	0.365	0.359	0.403	0.428
	Avg.	**0.217**	**0.254**	0.223	0.259	0.231	0.269	0.233	0.279	0.237	0.271	0.225	0.265	0.254	0.283	0.305	0.335	0.243	0.271	0.249	0.300	0.259	0.287	0.309	0.360
Electricity	96	**0.127**	0.231	0.135	0.230	0.137	0.237	0.134	0.233	0.139	0.238	0.131	**0.228**	0.129	0.234	0.147	0.248	0.147	0.251	0.140	0.237	0.168	0.272	0.193	0.308
	192	0.150	0.242	**0.149**	0.247	0.150	0.249	0.150	0.247	0.153	0.251	0.151	0.244	0.154	**0.227**	0.165	0.267	0.167	0.269	0.153	0.249	0.184	0.289	0.201	0.315
	336	**0.162**	**0.258**	0.167	0.266	0.168	0.266	0.165	0.264	0.169	0.266	0.167	0.262	0.165	0.262	0.178	0.279	0.174	0.275	0.169	0.267	0.198	0.300	0.214	0.329
	720	**0.198**	**0.279**	0.200	0.287	0.203	0.293	0.199	0.298	0.206	0.297	0.200	0.292	0.201	0.290	0.322	0.398	0.216	0.308	0.203	0.301	0.220	0.320	0.246	0.355
	Avg.	**0.159**	**0.253**	0.163	0.258	0.165	0.261	0.162	0.261	0.167	0.263	0.162	0.257	0.162	**0.253**	0.203	0.298	0.176	0.276	0.166	0.264	0.193	0.295	0.214	0.327
Traffic	96	**0.365**	**0.270**	0.379	0.274	0.380	0.277	0.366	0.279	0.388	0.282	0.387	0.278	0.368	0.277	0.367	0.288	0.394	0.389	0.410	0.282	0.593	0.321	0.587	0.366
	192	**0.372**	**0.281**	0.397	0.282	0.399	0.288	0.395	0.287	0.407	0.290	0.402	0.282	0.379	0.288	0.378	0.293	0.375	0.289	0.423	0.287	0.617	0.336	0.604	0.373
	336	**0.385**	**0.279**	0.407	0.289	0.408	0.290	0.406	0.283	0.412	0.294	0.413	0.288	0.397	0.292	0.389	0.294	0.395	0.283	0.436	0.296	0.629	0.336	0.621	0.383
	720	0.402	0.303	0.440	0.301	0.445	0.308	0.421	0.305	0.450	0.312	0.444	0.306	0.421	**0.298**	**0.401**	0.304	0.407	0.308	0.466	0.315	0.640	0.350	0.626	0.382
	Avg.	**0.381**	**0.283**	0.406	0.287	0.408	0.291	0.397	0.289	0.414	0.295	0.412	0.289	0.391	0.289	0.384	0.295	0.393	0.317	0.434	0.295	0.620	0.336	0.610	0.376
ETTh1	96	**0.360**	**0.388**	0.366	0.396	0.383	0.410	0.368	0.395	0.379	0.402	0.371	0.399	0.368	0.391	0.395	0.420	0.372	0.417	0.367	0.396	0.468	0.475	0.376	0.419
	192	**0.398**	**0.411**	0.401	0.420	0.419	0.435	0.404	0.415	0.424	0.403	0.420	0.429	0.417	0.427	0.441	0.418	0.432	0.401	0.419	0.484	0.485	0.420	0.448
	336	0.415	0.432	0.412	**0.431**	0.426	0.440	**0.408**	0.435	0.435	0.440	0.423	0.432	0.419	0.438	0.445	0.457	0.451	0.440	0.434	0.449	0.536	0.516	0.459	0.465
	720	0.436	**0.447**	0.440	0.458	**0.428**	0.456	0.439	0.503	0.441	0.459	0.452	0.461	0.446	0.465	0.537	0.530	0.476	0.458	0.472	0.493	0.593	0.537	0.506	0.507
	Avg.	**0.402**	**0.420**	0.405	0.426	0.414	0.435	0.405	0.437	0.418	0.431	0.412	0.428	0.416	0.428	0.451	0.462	0.429	0.437	0.419	0.439	0.520	0.503	0.440	0.460
ETTh2	96	**0.273**	0.331	0.278	0.340	0.297	0.357	0.282	**0.329**	0.289	0.347	0.279	0.343	0.274	0.335	0.304	0.360	0.287	0.331	0.301	0.367	0.376	0.415	0.358	0.397
	192	**0.335**	**0.372**	0.346	0.385	0.349	0.390	0.352	0.391	0.358	0.392	0.363	0.397	0.352	0.377	0.377	0.403	0.372	0.389	0.394	0.427	0.409	0.440	0.429	0.439
	336	**0.363**	**0.400**	0.367	0.406	0.373	0.408	0.382	0.403	0.383	0.414	0.381	0.419	0.369	0.427	0.405	0.429	0.407	0.423	0.506	0.495	0.425	0.455	0.496	0.487
	720	**0.396**	0.428	0.400	0.436	0.400	0.436	0.417	**0.425**	0.438	0.456	0.442	0.467	0.407	0.430	0.443	0.464	0.400	0.428	0.805	0.635	0.488	0.494	0.463	0.474
	Avg.	**0.342**	**0.383**	0.348	0.392	0.355	0.398	0.358	0.387	0.367	0.402	0.366	0.407	0.351	0.392	0.382	0.414	0.367	0.393	0.502	0.481	0.425	0.451	0.437	0.449
ETTm1	96	**0.285**	0.340	0.288	0.346	0.291	0.346	0.301	0.347	0.296	0.353	0.289	0.343	0.297	**0.338**	0.312	0.366	0.323	0.348	0.304	0.348	0.329	0.377	0.379	0.419
	192	**0.313**	**0.358**	0.323	0.365	0.336	0.373	0.331	0.371	0.335	0.373	0.329	0.366	0.333	0.367	0.347	0.385	0.368	0.369	0.336	0.367	0.371	0.401	0.426	0.441
	336	**0.355**	**0.377**	0.359	0.390	0.362	0.390	0.365	0.380	0.369	0.394	0.365	0.386	0.365	0.388	0.379	0.404	0.392	0.390	0.368	0.387	0.417	0.428	0.445	0.459
	720	0.405	**0.410**	**0.403**	0.418	0.410	0.421	0.423	0.422	0.418	0.424	0.423	0.417	0.425	0.431	0.441	0.442	0.469	0.433	0.421	0.418	0.483	0.464	0.543	0.490
	Avg.	**0.340**	**0.371**	0.343	0.380	0.350	0.383	0.355	0.380	0.355	0.386	0.352	0.378	0.355	0.381	0.370	0.399	0.388	0.385	0.357	0.380	0.400	0.418	0.448	0.452
ETTm2	96	**0.161**	**0.246**	0.165	0.257	0.184	0.275	0.167	0.261	0.170	0.264	0.168	0.258	0.168	0.256	0.179	0.271	0.168	0.254	0.168	0.263	0.201	0.286	0.203	0.287
	192	0.218	**0.284**	0.222	0.299	0.238	0.310	**0.214**	0.311	0.231	0.306	0.221	0.295	0.229	0.301	0.242	0.313	0.243	0.311	0.229	0.310	0.260	0.329	0.269	0.328
	336	**0.271**	**0.320**	0.277	0.330	0.286	0.340	0.284	0.325	0.280	0.339	**0.271**	0.327	0.281	0.334	0.288	0.344	0.299	0.338	0.289	0.352	0.331	0.376	0.325	0.366
	720	0.358	0.392	0.363	0.390	0.379	0.403	0.367	0.492	0.373	0.402	**0.355**	**0.381**	0.372	0.397	0.378	0.397	0.397	0.399	0.416	0.437	0.428	0.430	0.421	0.415
	Avg.	**0.252**	**0.311**	0.257	0.319	0.272	0.332	0.258	0.347	0.264	0.328	0.254	0.315	0.263	0.322	0.272	0.331	0.277	0.326	0.276	0.341	0.305	0.355	0.305	0.349

G.2 Short-Term Time Series Forecasting

Table 12 summarizes the full results of short-term time series forecasting. We can observe that MSH-LLM achieves the SOTA results on almost all datasets. Specifically, MSH-LLM performs slightly better than AutoTimes and S^2IP-LLM (i.e., 1.45% and 3.01% average SMAPE improvement), outperforming other latest baselines by a large margin (e.g., 6.68% and 8.13% average SMAPE improvement over Time-LLM and FPT, respectively).

Table 12: Full results of short-term time series forecasting. We follow the protocol of existing work (Pan et al., 2024) and set the input length to twice the output length. Lower values mean better performance. The best results are **bolded** and the second best results are underlined.

Methods		MSH-LLM (Ours)	AutoTimes* (NeurIPS 2024)	S^2IP-LLM (ICML 2024)	Time-LLM (ICLR 2024)	FPT (NeurIPS 2023)	iTransformer (ICLR 2024)	DLinear (AAAI 2023)	PatchTST (ICLR 2023)	N-HiTS (AAAI 2023)	N-BEATS (ICLR 2020)	TimesNet (ICLR 2023)
Year.	SMAPE	**13.305**	13.319	13.413	13.750	15.110	13.652	16.965	13.477	13.422	13.487	15.378
	MASE	2.995	**2.993**	3.024	3.055	3.565	3.095	4.283	3.019	3.056	3.036	3.554
	OWA	**0.784**	**0.784**	0.792	0.805	0.911	0.807	1.058	0.792	0.795	0.795	0.918
Quart.	SMAPE	**10.024**	10.101	10.352	10.671	10.597	10.353	12.145	10.380	10.185	10.564	10.465
	MASE	**1.146**	1.182	1.228	1.276	1.253	1.209	1.520	1.233	1.180	1.252	1.227
	OWA	**0.873**	0.890	0.922	0.950	0.938	0.911	1.106	0.921	0.893	0.936	0.923
Month.	SMAPE	**12.410**	12.710	12.995	13.416	13.258	13.079	13.514	12.959	13.059	13.089	13.513
	MASE	**0.912**	0.934	0.970	1.045	1.003	0.974	1.037	0.970	1.013	0.996	1.039
	OWA	**0.859**	0.880	0.910	0.957	0.931	0.911	0.956	0.905	0.929	0.922	0.957
Others.	SMAPE	4.721	4.843	4.805	4.973	6.124	4.780	6.709	4.952	**4.711**	6.599	6.913
	MASE	3.105	3.277	3.247	3.412	4.116	3.231	4.953	3.347	**3.054**	4.43	4.507
	OWA	0.986	1.026	1.017	1.053	1.259	1.012	1.487	1.049	**0.977**	1.393	1.438
Avg.	SMAPE	**11.659**	11.831	12.021	12.494	12.690	12.142	13.639	12.059	12.035	12.25	12.88
	MASE	**1.557**	1.585	1.612	1.731	1.808	1.631	2.095	1.623	1.625	1.698	1.836
	OWA	**0.837**	0.850	0.857	0.913	0.940	0.874	1.051	0.869	0.869	0.896	0.955

G.3 Time Series Classification

Table 13 summarizes the full results of time series classification. The baseline results are from existing works (Zhou et al., 2023a; Wu et al., 2022). From Table 13, we can observe that MSH-LLM achieves an average accuracy of 75.38%, surpassing all baselines including the best baseline FPT (74%) and TimesNet (73.6%).

Table 13: Full results of time series classification. We follow the protocol of existing work (Zhou et al., 2023a). The results are averaged from 10 subsets of UEA and higher values mean better performance. The best results are **bolded** and the second best results are underlined. # in the Transformers means the name of #former.

Methods	LLM4TS		Transformers									CNN		MLP		RNN		Classical methods	
	MSH-LLM	FPT	Trans#	Re#	In#	Pyra#	Auto#	Station#	FED#	ETS#	Flow#	TimesNet	TCN	DLinear	LightTS.	LSTNet	LSSL	XGBoost	Rocket
EthanolConcentration	36.2	34.2	32.7	31.9	31.6	30.8	31.6	32.7	31.2	28.1	33.8	35.7	28.9	32.6	29.7	39.9	31.1	43.7	**45.2**
FaceDetection	**69.7**	69.2	67.3	68.6	67	65.7	68.4	68	66	66.3	67.6	68.6	52.8	68	67.5	65.7	66.7	63.3	64.7
Handwriting	33.5	32.7	32	27.4	32.8	29.4	36.7	31.6	28	32.5	33.8	32.1	53.3	27	26.1	25.8	24.6	15.8	**58.8**
Heartbeat	**80.9**	77.2	76.1	77.1	80.5	75.6	74.6	73.7	73.7	71.2	77.6	78	75.6	75.1	75.1	77.1	72.7	73.2	75.6
JapaneseVowels	97.3	98.6	98.7	97.8	98.9	98.4	96.2	**99.2**	98.4	95.9	98.9	98.4	98.9	96.2	96.2	98.1	98.4	86.5	96.2
PEMS-SF	91.2	87.9	82.1	82.7	81.5	83.2	82.7	87.3	80.9	86	83.8	89.6	68.8	75.1	88.4	86.7	86.1	**98.3**	75.1
SelfRegulationSCP1	**93.5**	93.2	92.2	90.4	90.1	88.1	84	89.4	88.7	89.6	92.5	91.8	84.6	87.3	89.8	84	90.8	84.6	90.8
SelfRegulationSCP2	**59.8**	59.4	53.9	56.7	53.3	53.3	50.6	57.2	54.4	55	56.1	57.2	55.6	50.5	51.1	52.8	52.2	48.9	53.3
SpokenArabicDigits	99	99.2	98.4	97	**100**	99.6	**100**	**100**	**100**	**100**	98.8	99	95.6	81.4	**100**	**100**	**100**	69.6	71.2
UWaveGestureLibrary	92.7	88.1	85.6	85.6	85.6	83.4	85.9	87.5	85.3	85	86.6	85.3	88.4	82.1	80.3	87.8	85.9	75.9	**94.4**
Average	**75.38**	74	71.9	71.5	72.1	70.8	71.1	72.7	70.7	71	73	73.6	70.3	67.5	70.4	71.8	70.9	66	72.5

G.4 Few-Shot Learning

Table 14 and Table 15 summarize the results of few-shot learning under 10% training data. In the scope of 10% few-shot learning, MSH-LLM achieves SOTA results in almost all cases. Specifically, MSH-LLM achieves an average error reduction of 7.32% and 3.95% compared to LLM4TS methods (i.e., S^2IP-LLM and Time-LLM) in MSE and MAE, respectively, and outperforms the latest training from scratch method iTransformer by 24.85% and 20.03% in MSE and MAE, respectively. Table 16 summarizes the average results and full results of few-shot learning under 5% training data. We can observe that MSH-LLM still achieves SOTA results even with fewer training data. Specifically, MSH-LLM achieves an average error reduction of 10.47% and 6.74% compared to LLM4TS methods (i.e., S^2IP-LLM and Time-LLM) in MSE and MAE, respectively.

Table 14: Few-shot learning results under 10% training data setting. Results are averaged from all forecasting lengths. The best results are **bolded** and the second best results are underlined. Full results are listed in Appendix G.4, Table15.

Methods	MSH-LLM (Ours)		S^2IP-LLM (ICML 2024)		Time-LLM (ICLR 2024)		FPT (NeurIPS 2023)		iTransformer (ICLR 2024)		PatchTST (ICLR 2023)		TimesNet (ICLR 2023)		FEDformer (ICML 2022)		NSFormer (NeurIPS 2022)		ETSformer (arXiv 2022)		Autoformer (NeurIPS 2021)	
Metric	MSE	MAE	MSE	MAE	MSE	MAE	MSE	MAE	MSE	MAE	MSE	MAE	MSE	MAE	MSE	MAE	MSE	MAE	MSE	MAE	MSE	MAE
Weather	**0.230**	**0.267**	0.233	0.272	0.237	0.275	0.238	0.275	0.308	0.338	0.242	0.279	0.279	0.301	0.284	0.324	0.318	0.323	0.318	0.360	0.300	0.342
Electricity	**0.167**	**0.260**	0.175	0.271	0.177	0.273	0.176	0.269	0.196	0.293	0.180	0.273	0.323	0.392	0.346	0.427	0.444	0.480	0.660	0.617	0.431	0.478
Traffic	**0.423**	**0.296**	0.427	0.307	0.429	0.307	0.440	0.310	0.495	0.361	0.430	0.305	0.951	0.535	0.663	0.425	1.453	0.815	1.914	0.936	0.749	0.446
ETTh1	**0.563**	**0.514**	0.593	0.529	0.785	0.553	0.590	0.525	0.910	0.860	0.633	0.542	0.869	0.628	0.639	0.561	0.915	0.639	1.180	0.834	0.702	0.596
ETTh2	**0.392**	0.423	0.419	0.439	0.424	0.441	0.397	**0.421**	0.489	0.483	0.415	0.431	0.479	0.465	0.466	0.475	0.462	0.455	0.894	0.713	0.488	0.499
ETTm1	**0.403**	**0.424**	0.455	0.435	0.487	0.461	0.464	0.441	0.728	0.565	0.501	0.466	0.677	0.537	0.722	0.605	0.797	0.578	0.980	0.714	0.802	0.628
ETTm2	**0.280**	**0.327**	0.284	0.332	0.305	0.344	0.293	0.335	0.336	0.373	0.296	0.343	0.320	0.353	0.463	0.488	0.332	0.366	0.447	0.487	1.342	0.930

Table 15: Full results of few-shot learning under 10% training data. We follow the same protocol of existing work (Pan et al., 2024). The input length is set to 512, and the forecasting lengths are set to 96, 192, 336, and 720. Lower values mean better performance. The best results are **bolded** and the second best results are underlined.

Methods		MSH-LLM (Ours)		S^2IP-LLM (ICML 2024)		Time-LLM (ICLR 2024)		FPT (NeurIPS 2023)		iTransformer (ICLR 2024)		PatchTST (ICLR 2024)		TimesNet (ICLR 2023)		FEDformer (ICML 2022)		NSFormer (NeurIPS 2022)		ETSformer (arXiv 2022)		Autoformer (NeurIPS 2021)	
Metric		MSE	MAE	MSE	MAE	MSE	MAE	MSE	MAE	MSE	MAE	MSE	MAE	MSE	MAE	MSE	MAE	MSE	MAE	MSE	MAE	MSE	MAE
Weather	96	**0.152**	**0.208**	0.159	0.210	0.160	0.213	0.163	0.215	0.253	0.307	0.165	0.215	0.184	0.230	0.188	0.253	0.192	0.234	0.199	0.272	0.221	0.297
	192	0.206	**0.248**	**0.200**	0.251	0.204	0.254	0.210	0.254	0.292	0.328	0.210	0.257	0.245	0.283	0.250	0.304	0.269	0.295	0.279	0.332	0.270	0.322
	336	**0.252**	**0.286**	0.257	0.293	0.255	0.291	0.256	0.292	0.322	0.346	0.259	0.297	0.305	0.321	0.312	0.346	0.370	0.357	0.356	0.386	0.320	0.351
	720	**0.311**	**0.326**	0.317	0.335	0.329	0.345	0.321	0.339	0.365	0.374	0.332	0.346	0.381	0.371	0.387	0.393	0.441	0.405	0.437	0.448	0.390	0.396
	Avg	**0.230**	**0.267**	0.233	0.272	0.237	0.275	0.238	0.275	0.308	0.338	0.242	0.279	0.279	0.301	0.284	0.324	0.318	0.323	0.318	0.360	0.300	0.342
Electricity	96	0.139	**0.235**	0.143	0.243	**0.137**	0.240	0.139	0.237	0.154	0.257	0.140	0.238	0.299	0.373	0.231	0.323	0.420	0.466	0.599	0.587	0.261	0.348
	192	**0.153**	**0.248**	0.159	0.258	0.159	0.258	0.156	0.252	0.171	0.272	0.160	0.255	0.305	0.379	0.261	0.356	0.411	0.459	0.620	0.598	0.338	0.406
	336	**0.169**	**0.263**	0.170	0.269	0.181	0.278	0.175	0.270	0.196	0.295	0.180	0.276	0.319	0.391	0.360	0.445	0.434	0.473	0.662	0.619	0.410	0.474
	720	**0.207**	**0.295**	0.230	0.315	0.232	0.317	0.233	0.317	0.263	0.348	0.241	0.323	0.369	0.426	0.530	0.585	0.510	0.521	0.757	0.664	0.715	0.685
	Avg	**0.167**	**0.260**	0.175	0.271	0.177	0.273	0.176	0.269	0.196	0.293	0.180	0.273	0.323	0.392	0.346	0.427	0.444	0.480	0.660	0.617	0.431	0.478
Traffic	96	0.405	**0.286**	**0.403**	0.293	0.406	0.295	0.414	0.297	0.448	0.329	**0.403**	0.289	0.719	0.416	0.639	0.400	1.412	0.802	1.643	0.855	0.672	0.405
	192	0.415	**0.286**	**0.412**	0.295	0.416	0.300	0.426	0.301	0.487	0.360	0.415	0.296	0.748	0.428	0.637	0.416	1.419	0.806	1.641	0.854	0.727	0.424
	336	**0.417**	**0.293**	0.427	0.316	0.430	0.309	0.434	0.303	0.514	0.372	0.426	0.304	0.853	0.471	0.655	0.427	1.443	0.815	1.711	0.878	0.749	0.454
	720	**0.453**	**0.319**	0.469	0.325	0.467	0.324	0.487	0.337	0.532	0.383	0.474	0.331	1.485	0.825	0.722	0.456	1.539	0.837	2.660	1.157	0.847	0.499
	Avg	**0.423**	**0.296**	0.427	0.307	0.429	0.307	0.440	0.310	0.495	0.361	0.430	0.305	0.951	0.535	0.663	0.425	1.453	0.815	1.914	0.936	0.749	0.446
ETTh1	96	0.460	**0.450**	0.481	0.474	0.720	0.533	**0.458**	0.456	0.790	0.586	0.516	0.485	0.861	0.628	0.512	0.499	0.918	0.639	1.112	0.806	0.613	0.552
	192	**0.516**	**0.488**	0.518	0.491	0.747	0.545	0.570	0.516	0.837	0.609	0.598	0.524	0.797	0.593	0.624	0.555	0.915	0.629	1.155	0.823	0.722	0.598
	336	**0.594**	0.537	0.664	0.570	0.793	0.551	0.608	**0.535**	0.780	0.575	0.657	0.550	0.941	0.648	0.691	0.574	0.939	0.644	1.179	0.832	0.750	0.619
	720	**0.680**	**0.581**	0.711	0.584	0.880	0.584	0.725	0.591	1.234	0.811	0.762	0.610	0.877	0.641	0.728	0.614	0.887	0.645	1.273	0.874	0.721	0.616
	Avg	**0.563**	**0.514**	0.593	0.529	0.785	0.553	0.590	0.525	0.910	0.860	0.633	0.542	0.869	0.628	0.639	0.561	0.915	0.639	1.180	0.834	0.702	0.596
ETTh2	96	**0.331**	**0.366**	0.354	0.400	0.334	0.381	**0.331**	0.374	0.404	0.435	0.353	0.389	0.378	0.409	0.382	0.416	0.389	0.411	0.678	0.619	0.413	0.451
	192	**0.374**	0.414	0.401	0.423	0.430	0.438	0.402	**0.411**	0.470	0.474	0.403	0.414	0.490	0.467	0.478	0.474	0.473	0.455	0.785	0.666	0.474	0.477
	336	**0.396**	**0.432**	0.442	0.450	0.449	0.458	0.406	0.433	0.489	0.485	0.426	0.441	0.537	0.494	0.504	0.501	0.477	0.472	0.839	0.694	0.547	0.543
	720	0.465	0.478	0.480	0.486	0.485	0.490	**0.449**	**0.464**	0.593	0.538	0.477	0.480	0.510	0.491	0.499	0.509	0.507	0.480	1.273	0.874	0.516	0.523
	Avg	**0.392**	0.423	0.419	0.439	0.424	0.441	0.397	**0.421**	0.489	0.483	0.415	0.431	0.479	0.465	0.466	0.475	0.462	0.455	0.894	0.713	0.488	0.499
ETTm1	96	**0.349**	**0.383**	0.388	0.401	0.412	0.422	0.390	0.404	0.709	0.556	0.410	0.419	0.583	0.501	0.578	0.518	0.761	0.568	0.911	0.688	0.774	0.614
	192	**0.377**	**0.410**	0.422	0.421	0.447	0.438	0.429	0.423	0.717	0.548	0.437	0.434	0.630	0.528	0.617	0.546	0.781	0.574	0.955	0.703	0.754	0.592
	336	**0.405**	0.434	0.456	**0.430**	0.497	0.465	0.469	0.439	0.735	0.575	0.476	0.454	0.725	0.568	0.998	0.775	0.803	0.587	0.991	0.719	0.869	0.677
	720	**0.482**	**0.468**	0.554	0.490	0.594	0.521	0.569	0.498	0.752	0.584	0.681	0.556	0.769	0.549	0.693	0.579	0.844	0.581	1.062	0.747	0.810	0.630
	Avg	**0.403**	**0.424**	0.455	0.435	0.487	0.461	0.464	0.441	0.728	0.565	0.501	0.466	0.677	0.537	0.722	0.605	0.797	0.578	0.980	0.714	0.802	0.628
ETTm2	96	**0.178**	**0.261**	0.192	0.274	0.224	0.296	0.188	0.269	0.245	0.322	0.191	0.274	0.212	0.285	0.291	0.399	0.229	0.308	0.331	0.430	0.352	0.454
	192	**0.238**	**0.304**	0.246	0.313	0.260	0.317	0.251	0.309	0.274	0.338	0.252	0.317	0.270	0.323	0.307	0.379	0.291	0.343	0.400	0.464	0.694	0.691
	336	**0.299**	0.341	0.301	**0.340**	0.312	0.349	0.307	0.346	0.361	0.394	0.306	0.353	0.323	0.353	0.543	0.559	0.348	0.376	0.469	0.498	2.408	1.407
	720	0.403	**0.401**	**0.400**	0.403	0.424	0.416	0.426	0.417	0.467	0.442	0.433	0.427	0.474	0.449	0.712	0.614	0.461	0.438	0.589	0.557	1.913	1.166
	Avg	**0.280**	**0.327**	0.284	0.332	0.305	0.344	0.293	0.335	0.336	0.373	0.296	0.343	0.320	0.353	0.463	0.488	0.332	0.366	0.447	0.487	1.342	0.930

Table 16: Full results of few-shot learning under 5% training data. We follow the same protocol of existing work (Pan et al., 2024). The input length is set to 512, and the forecasting lengths are set to 96, 192, 336, and 720. '- -' indicates 5% training data is insufficient to constitute a training set. The best results are **bolded** and the second best results are underlined.

Methods		MSH-LLM (Ours)		S^2IP-LLM (ICML 2024)		Time-LLM (ICLR 2024)		FPT (NeurIPS 2023)		iTransformer (ICLR 2024)		PatchTST (ICLR 2024)		TimesNet (ICLR 2023)		FEDformer (ICML 2022)		NSFormer (NeurIPS 2022)		ETSformer (arXiv 2022)		Autoformer (NeurIPS 2021)	
Metric		MSE	MAE	MSE	MAE	MSE	MAE	MSE	MAE	MSE	MAE	MSE	MAE	MSE	MAE	MSE	MAE	MSE	MAE	MSE	MAE	MSE	MAE
Weather	96	**0.170**	**0.214**	0.175	0.228	0.176	0.230	0.175	0.230	0.264	0.307	0.171	0.224	0.207	0.253	0.229	0.309	0.215	0.252	0.218	0.295	0.227	0.299
	192	**0.213**	**0.253**	0.225	0.271	0.226	0.275	0.227	0.276	0.284	0.326	0.230	0.277	0.272	0.307	0.265	0.317	0.290	0.307	0.294	0.331	0.278	0.333
	336	**0.259**	**0.289**	0.282	0.321	0.292	0.325	0.286	0.322	0.323	0.349	0.294	0.326	0.313	0.328	0.353	0.392	0.353	0.348	0.359	0.398	0.351	0.393
	720	**0.346**	**0.367**	0.361	0.371	0.364	0.375	0.366	0.379	0.366	0.375	0.384	0.387	0.400	0.385	0.391	0.394	0.452	0.407	0.461	0.461	0.387	0.389
	Avg	**0.247**	**0.281**	0.260	0.297	0.264	0.301	0.263	0.301	0.309	0.339	0.269	0.303	0.298	0.318	0.309	0.353	0.327	0.328	0.333	0.371	0.310	0.353
Electricity	96	0.144	0.243	0.148	0.248	0.148	0.248	**0.143**	**0.241**	0.162	0.264	0.145	0.244	0.315	0.389	0.235	0.322	0.484	0.518	0.697	0.638	0.297	0.367
	192	**0.158**	**0.255**	0.159	**0.255**	0.160	0.257	0.159	**0.255**	0.180	0.278	0.163	0.260	0.318	0.396	0.247	0.341	0.501	0.531	0.718	0.648	0.308	0.375
	336	0.177	0.272	**0.175**	**0.271**	0.183	0.282	0.179	0.274	0.207	0.305	0.183	0.281	0.340	0.415	0.267	0.356	0.574	0.578	0.758	0.667	0.354	0.411
	720	**0.217**	**0.304**	0.235	0.326	0.236	0.329	0.233	0.323	0.258	0.339	0.233	0.323	0.635	0.613	0.318	0.394	0.952	0.786	1.028	0.788	0.426	0.466
	Avg	**0.174**	**0.269**	0.179	0.275	0.181	0.279	0.178	0.273	0.201	0.296	0.181	0.277	0.402	0.453	0.266	0.353	0.627	0.603	0.800	0.685	0.346	0.404
Traffic	96	0.405	**0.273**	0.410	0.288	0.414	0.293	0.419	0.298	0.431	0.312	**0.404**	0.286	0.854	0.492	0.670	0.421	1.468	0.821	1.643	0.855	0.795	0.481
	192	**0.405**	**0.291**	0.416	0.298	0.419	0.300	0.434	0.305	0.456	0.326	0.412	0.294	0.894	0.517	0.653	0.405	1.509	0.838	1.856	0.928	0.837	0.503
	336	**0.428**	0.312	0.435	0.313	0.438	0.315	0.449	0.313	0.465	0.334	0.439	**0.310**	0.853	0.471	0.707	0.445	1.602	0.860	2.080	0.999	0.867	0.523
	720	- -	- -	- -	- -	- -	- -	- -	- -	- -	- -	- -	- -	- -	- -	- -	- -	- -	- -	- -	- -	- -	- -
	Avg	**0.413**	**0.292**	0.420	0.299	0.423	0.302	0.434	0.305	0.450	0.324	0.418	0.296	0.867	0.493	0.676	0.423	1.526	0.839	1.859	0.927	0.833	0.502
ETTh1	96	**0.489**	**0.475**	0.500	0.493	0.732	0.556	0.543	0.506	0.808	0.610	0.557	0.519	0.892	0.625	0.593	0.529	0.952	0.650	1.169	0.832	0.681	0.570
	192	0.658	**0.535**	0.690	0.539	0.872	0.604	0.748	0.580	0.928	0.658	0.711	0.570	0.940	0.665	**0.652**	0.563	0.943	0.645	1.221	0.853	0.725	0.602
	336	0.738	0.600	0.761	0.620	1.071	0.721	0.754	0.595	1.475	0.861	0.816	0.619	0.945	0.653	**0.731**	**0.594**	0.935	0.644	1.179	0.832	0.761	0.624
	720	- -	- -	- -	- -	- -	- -	- -	- -	- -	- -	- -	- -	- -	- -	- -	- -	- -	- -	- -	- -	- -	- -
	Avg	**0.628**	**0.537**	0.650	0.550	0.891	0.627	0.681	0.560	1.070	0.710	0.694	0.569	0.925	0.647	0.658	0.562	0.943	0.646	1.189	0.839	0.722	0.598
ETTh2	96	**0.342**	**0.389**	0.363	0.409	0.399	0.420	0.376	0.421	0.397	0.427	0.401	0.421	0.409	0.420	0.390	0.424	0.408	0.423	0.678	0.619	0.428	0.468
	192	**0.375**	0.412	**0.375**	**0.411**	0.487	0.479	0.418	0.441	0.438	0.445	0.452	0.455	0.483	0.464	0.457	0.465	0.497	0.468	0.845	0.697	0.496	0.504
	336	**0.401**	**0.419**	0.403	0.421	0.858	0.660	0.408	0.439	0.631	0.553	0.464	0.469	0.499	0.479	0.477	0.483	0.507	0.481	0.905	0.727	0.486	0.496
	720	- -	- -	- -	- -	- -	- -	- -	- -	- -	- -	- -	- -	- -	- -	- -	- -	- -	- -	- -	- -	- -	- -
	Avg	**0.373**	**0.407**	0.380	0.413	0.581	0.519	0.400	0.433	0.488	0.475	0.827	0.615	0.439	0.448	0.463	0.454	0.470	0.489	0.809	0.681	0.441	0.457
ETTm1	96	**0.328**	**0.365**	0.357	0.390	0.422	0.424	0.386	0.405	0.589	0.510	0.399	0.414	0.606	0.518	0.628	0.544	0.823	0.587	1.031	0.747	0.726	0.578
	192	**0.353**	**0.395**	0.432	0.434	0.448	0.440	0.440	0.438	0.703	0.565	0.441	0.436	0.681	0.539	0.666	0.566	0.844	0.591	1.087	0.766	0.750	0.591
	336	**0.394**	**0.412**	0.440	0.442	0.519	0.482	0.485	0.459	0.898	0.641	0.499	0.467	0.786	0.597	0.807	0.628	0.870	0.603	1.138	0.787	0.851	0.659
	720	**0.518**	**0.483**	0.593	0.521	0.708	0.573	0.577	0.499	0.948	0.671	0.767	0.587	0.796	0.593	0.822	0.633	0.893	0.611	1.245	0.831	0.857	0.655
	Avg	**0.398**	**0.414**	0.455	0.446	0.524	0.479	0.472	0.450	0.784	0.596	0.526	0.476	0.717	0.561	0.730	0.592	0.857	0.598	1.125	0.782	0.796	0.620
ETTm2	96	**0.179**	**0.264**	0.197	0.278	0.225	0.300	0.199	0.280	0.265	0.339	0.206	0.288	0.220	0.299	0.229	0.320	0.238	0.316	0.404	0.485	0.232	0.322
	192	**0.242**	**0.309**	0.254	0.322	0.275	0.334	0.256	0.316	0.310	0.362	0.264	0.324	0.311	0.361	0.394	0.361	0.298	0.349	0.479	0.521	0.291	0.357
	336	**0.300**	**0.344**	0.315	0.350	0.339	0.371	0.318	0.353	0.373	0.399	0.334	0.367	0.338	0.366	0.378	0.427	0.353	0.380	0.552	0.555	0.478	0.517
	720	**0.411**	**0.414**	0.421	0.421	0.464	0.441	0.460	0.436	0.478	0.454	0.454	0.432	0.509	0.465	0.523	0.510	0.475	0.445	0.701	0.627	0.553	0.538
	Avg	**0.283**	**0.333**	0.296	0.342	0.325	0.361	0.308	0.346	0.356	0.388	0.314	0.352	0.344	0.372	0.381	0.404	0.341	0.372	0.534	0.547	0.388	0.433

G.5 Zero-Shot Learning

The zero-shot learning experiment is conducted on two distinct datasets, i.e., the source dataset and the target dataset, where the model is trained on the source dataset and tested on the target dataset without fine-tuning. Following existing works (Zhou et al., 2023a; Liu et al., 2024), we use M3 and M4 datasets to evaluate the zero-shot capabilities of the models.

For M4 $\rightarrow$ M3, which means training on M4 dataset and testing on M3 dataset, we directly utilize the M4 model trained in short-term forecasting experiments. Due to the varying forecasting lengths across different subsets, we use models trained on the corresponding subsets of M4 to test on M3 Yearly, M3 Quarterly, and M3 Monthly. For M3 Others, we use the model trained on M4 Quarterly to maintain the same forecasting lengths.

For M3 $\rightarrow$ M4, similarly, for M4 Yearly, M4 Quarterly, and M4 Monthly, we directly employ models trained on corresponding subsets of M3 for testing. For the remaining subsets, M4 Weekly, M4 Daily, and M4 Hourly, we perform inference using the model trained on M3 Monthly, following the settings of existing works (Zhou et al., 2023a; Liu et al., 2024).

Table 17: Full results of zero-shot learning. We adopt the same protocol of existing work (Pan et al., 2024). M4→M3 means training on M4 datasets and testing on M3 datasets, and vice versa. Lower SMAPE means better performance. The best results are **bolded** and the second best results are underlined.

Method		MSH-LLM (Ours)	AutoTimes (NeurIPS 2024)	FPT (NeurIPS 2023)	DLinear (AAAI 2023)	PatchTST (ICLR 2023)	TimesNet (ICLR 2023)	NSformer (NeurIPS 2022)	FEDformer (ICML 2022)	Informer (AAAI 2021)	Reformer (ICLR 2019)
M4 → M3	Yearly	**15.650**	15.710	16.420	17.430	15.990	18.750	17.050	16.000	19.700	16.030
	Quarterly	**9.240**	9.350	10.130	9.740	9.620	12.260	12.560	9.480	13.000	9.760
	Monthly	**13.570**	14.060	14.100	15.650	14.710	14.010	16.820	15.120	15.910	14.800
	Others	5.663	5.790	**4.810**	6.810	9.440	6.880	8.130	8.940	13.030	7.530
	Average	**12.469**	12.750	13.060	14.030	13.390	14.170	15.290	13.530	15.820	13.370
M3 → M4	Yearly	**13.645**	13.728	13.740	14.193	13.966	15.655	14.988	13.887	18.542	15.652
	Quarterly	**10.703**	10.742	10.787	18.856	10.929	11.877	11.686	11.513	16.907	11.051
	Monthly	**14.489**	14.558	14.630	14.765	14.664	16.165	16.098	18.154	23.454	15.604
	Others	**6.132**	6.259	7.081	9.194	7.087	6.863	6.977	7.529	7.348	7.001
	Average	**12.968**	13.036	13.125	15.337	13.228	14.553	14.327	15.047	19.047	14.092

Table 17 summarizes the full results of zero-shot learning. MSH-LLM remarkably surpasses all other baselines in zero-shot learning. Specifically, we observe over 10.23% SMAPE error reductions across all baselines on average. Our improvements are consistently significant on typical scenarios

(e.g., M4→M3 Others and M3→M4 Others), with over 23.04% and 14.72% average SMAPE error reductions, respectively. We attribute this to the successful utilization of transfer learning capabilities in LLMs.

H Ablation Studies

Multi-Scale Extraction (ME) Module. To investigate the effectiveness of the ME module, we conduct an ablation study by carefully designing the following variant:

-w/o ME: Removing the multi-scale extraction module and only performs alignment between input time series and text prototypes.

Table 18: The results of different ME module and hyperedging mechanism on ETTh1 dataset. The best results are **bolded**.

Methods	-w/o ME		-w/o HM		-PM		MSH-LLM	
Metirc	MSE	MAE	MSE	MAE	MSE	MAE	MSE	MAE
96	0.412	0.400	0.693	0.560	0.380	0.392	**0.360**	**0.388**
192	0.413	0.412	0.751	0.513	0.405	0.424	**0.398**	**0.411**
336	0.421	0.436	0.756	0.596	0.423	0.443	**0.415**	**0.432**

The experimental results on ETTh1 dataset are shown in Table 18. We can observe that MSH-LLM performs better than -w/o ME, showing the effectiveness of the ME module. The reason is that the ME module can provide richer representations than relying solely on single-scale alignment.

Hyperedging Mechanism. To investigate the effect of the hyperedging mechanism, we conduct an ablation study by carefully designing the following two variants:

-w/o HM: Removing the hyperedging mechanism and directly performing alignment between temporal features and text prototypes at different scales.

-PM: Replacing the hyperedging mechanism with the patching mechanism.

The experimental results on ETTh1 dataset are shown in Table 18. We can observe that MSH-LLM performs better than -w/o HM and -PM, demonstrating the effectiveness of our hyperedging mechanism in enhancing the semantic information of time series semantic space. In addition, we can observe that -w/o HM achieves the worst performance, the reason is that the individual time point or temporal feature contains less semantic information, making it hard to align with the informative semantic space of natural language.

Multi-Scale Text Prototypes Extraction. To investigate the impact of different multi-scale text prototypes extraction, we conduct an ablation study by designing the following two variants:

R.1: Replacing word token embeddings based on pre-trained LLMs with word token embeddings generated from manually select word and phrase descriptions (e.g., small, big, rapid increase, and steady decrease).

R.2: Replacing word token embeddings based on pre-trained LLMs with word token embeddings generated from randomly selected word and phrase descriptions (e.g., increase, happy, can, and white noise).

Table 19: The results of different multi-scale text prototypes extraction and CMA module on ETTh1 dataset. The best results are **bolded**.

Methods	R.1		R.2		R.3		P.1		-ASO		MSH-LLM	
Metric	MSE	MAE	MSE	MAE	MSE	MAE	MSE	MAE	MSE	MAE	MSE	MAE
96	0.467	0.467	0.441	0.447	0.697	0.561	0.363	0.390	0.396	0.413	**0.360**	**0.388**
192	0.497	0.483	0.475	0.467	0.760	0.600	0.405	0.417	0.417	0.428	**0.398**	**0.411**
336	0.517	0.496	0.514	0.489	0.787	0.609	0.417	**0.424**	0.433	0.442	**0.415**	0.432

The experimental results on ETTh1 dataset are shown in Table 19, from which we can observe that MSH-LLM performs better than R.1 and R.2 by a large margin, which indicates the effectiveness

of our multi-scale text prototype extraction than approaches of manually selecting. In addition, it is notable that we initially assumed that aligning multi-scale temporal features with relevant natural language descriptions (e.g., small, big, rapid increase, and steady decrease) can offer better performance. However, the experimental results show that word token embeddings generated from randomly selected word and phrase descriptions achieve better performance than R.1. The reason is that the aligned word token embeddings may not be fully related to time series. Actually, LLMs can function as pattern recognition machines (Sun et al., 2024; Zhou et al., 2023a), and we believe the text prototypes matched by LLMs can better match temporal patterns, even they may not be fully related to time series.

CMA Module. To investigate the effectiveness of the cross-modality alignment module, we conduct an ablation study by designing the following two variants:

R.3: Removing the CMA module and directly concatenating the hyperedge features with MoP before feeding them into LLMs to obtain the output representations.

P.1: Performing detailed cross-modality alignment across all scales.

The experimental results on ETTh1 dataset are shown in Table 19, from which we can observe that MSH-LLM performs significantly better than R.3, showing the effectiveness of the CMA module. The reason is that the CMA module can help align the semantic space of natural language and that of time series. In addition, we can observe that MSH-LLM outperforms P.1 in most cases. This is because performing detailed alignment across all scales may introduce redundant information interference.

In addition, it has been shown that treating cross-modality alignment as an independent task (Li et al., 2023) can help the model focus more on the alignment objective and may potentially improve model performance. To investigate the impact of different cross-modality alignment strategy, we conduct ablation studies on the ETTh1 dataset by carefully designing the following variant:

-ASO: This approach treats cross-modality alignment as a standalone objective and employs a two-stage training strategy for time series analysis. The detailed design of the objective function are formulated as follows:

Specifically, for the given hyperedge feature $\boldsymbol{e}_j^s$ and text prototypes $\boldsymbol{u}_j^s$ at scale s, we first we first compute both the cosine similarity and the Euclidean distance between them. The cosine similarity can be formulated as follows:

$$\tau_{i,j} = \frac{\boldsymbol{e}_i^s (\boldsymbol{e}_j^s)^T}{\|\boldsymbol{e}_i^s\|_2 \left\|\boldsymbol{e}_j^s\right\|_2}, \tag{14}$$

where . denotes the dot product and $||.||_2$ represents the L2 norm. The Euclidean distance can be defined as:

$$D_{i,j} = \|\boldsymbol{e}_i^s - \boldsymbol{u}_j^s\|_2 = \sqrt{\sum_{d=1}^{D} ((\boldsymbol{e}_i^s)^d - (\boldsymbol{u}_j^s)^d)^2} \tag{15}$$

Then, the loss function L_{aso}^s at scale s based on the correlation weight and Euclidean distance can be formulated as follows:

$$L_{aso}^s = \frac{1}{(M^s)^2} \sum_{i=1}^{M^s} \sum_{j=1}^{M^s} \left(\tau_{i,j} D_{i,j} + (1 - \tau_{i,j}) max(\gamma - D_{i,j}, 0)\right), \tag{16}$$

where $\gamma > 0$ denotes the threshold. Notably, when $\tau_{i,j} = 1$, indicating that e_i^s and u_k^s are deemed similar, the loss turns to $L_{aso} = \frac{1}{(M^s)^2} \sum_{i=1}^{M^s} \sum_{j=1}^{M^s} \tau_{i,j} D_{i,j}$, where the loss will increase if $D_{i,j}$ becomes large. Conversely, when $\alpha_{i,j} = 0$, meaning e_i and e_k are regarded as dissimilar, the loss turns to $L_{aso} = \frac{1}{(M^s)^2} \sum_{i=1}^{M^s} \sum_{j=1}^{M^s} (1 - \tau_{i,j}) max(\gamma - D_{i,j}, 0)$, where the loss will increase if $D_{i,j}$ falls below the threshold and turns smaller. Other cases lie between the above circumstances. The final loss function can be formulated as follows:

$$L = \sum_{s=1}^{S} L_{aso}^s, \tag{17}$$

The experimental results are shown in Table 19. We can observe that MSH-LLM performs better than -ASO in most cases. We attribute the performance drop to the following two aspects: 1) Treating

cross-modality alignment as a standalone objective, the model may lack supervision signals from the primary time series analysis task, thereby missing the potential synergy with the main task. 2) Unlike CV or NLP, time series datasets often contain limited training samples, which may result in insufficient generalization capability when cross-modality alignment is trained independently as a standalone objective. The experimental results show the effectiveness of our CMA module.

LLM backbones. To investigate the effectiveness of LLM backbones for time series analysis, we conduct an ablation study by designing the following two variants:

-w/o LLM: Removing the LLM backbones and directly feeding the connected multi-scale temporal features into the linear mapping layer.

-LLM2Attn: Replacing the LLM backbones with a single multi-head attention layer.

Table 20: The results of LLM backbone variants on ETTh1 dataset. The best results are **bolded**.

Methods	-w/o LLM		-LLM2Attn		MSH-LLM	
Metric	MSE	MAE	MSE	MAE	MSE	MAE
96	0.401	0.437	0.381	0.405	**0.360**	**0.388**
192	0.435	0.447	0.415	0.423	**0.398**	**0.411**
336	0.441	0.453	0.421	0.437	**0.415**	**0.432**

The experimental results on ETTh1 dataset are shown in Table 20, from which we can observe that MSH-LLM performs better than -w/o LLM and -LLM2Attn, demonstrating the effectiveness of LLM backbones for time series analysis.

Data-Correlated Prompts. To quantify the impact of endogenous data-correlated prompts on the final performance, we have newly added ablation studies by carefully designing the following variants:

-TV: It replaces the data-correlated prompts with the prompt template used in Time-LLM.

-SD1: It incorporates more data statistics (e.g., trends, lags, means, and standard deviation) into the data-correlated prompts.

-SD2: It selects a few key statistical metrics to include as data statistics in the data-correlated prompts.

-TG: It incorporates different temporal granularity information into the data-correlated prompts.

Table 21: The results of different multi-scale text prototypes extraction and CMA module on ETTh1 dataset. The best results are **bolded**.

Methods	-TV		-SD1		-SD2		-TG		MSH-LLM	
Metric	MSE	MAE	MSE	MAE	MSE	MAE	MSE	MAE	MSE	MAE
96	0.363	0.389	0.360	0.389	**0.358**	**0.388**	0.359	0.390	0.360	0.388
192	0.398	0.413	0.400	0.411	0.397	0.413	0.398	0.413	**0.398**	**0.411**
336	0.417	0.435	0.415	0.433	0.414	**0.431**	**0.413**	0.432	0.415	0.432

The experimental results are shown in Table 21. From Table 21, we can obtain the following tendencies: 1) MSH-LLM performs better than -TV in most cases, showing the effectiveness of our prompt template. 2) -SD2 outperforms both -SD1 and MSH-LLM, suggesting that more statistical features do not necessarily lead to better performance, and carefully selected statistical metrics may yield superior results. 3) MSH-LLM achieves comparable performance to these variants. The reason is that we design the mixture of prompts (MoP) mechanism, which mitigates the impact of relying on a single prompt or specific statistical features. The experimental results demonstrate the robustness of our MoP mechanism.

Capability-Enhancing Prompts. To investigate the impact of the logical thinking prompt and time series reasoning correlated prompt used in capability-enhancing prompts, we conduct ablation studies by carefully designing the following variants:

-w/o LR: It removes the logical thinking prompt used in the MoP mechanism.

-w/o TSR: It removes the time series reasoning correlated prompt used in the MoP mechanism.

Table 22: The results of different capability-enhancing prompts. The best results are **bolded**.

Methods	-w/o LR		-w/o TSR		MSH-LLM	
Metric	MSE	MAE	MSE	MAE	MSE	MAE
96	0.372	0.274	0.370	0.268	**0.365**	**0.270**
192	0.389	0.287	0.383	0.283	**0.372**	**0.281**
336	0.390	0.282	0.379	0.280	**0.385**	**0.279**

The experimental results on Traffic dataset are shown in Table 22. From Table 22, we can observe that -w/o LR performs better than -w/o TSR, indicating that the logical reasoning prompt plays a more critical role than the time series reasoning correlated prompt. In addition, -w/o LR and -w/o TSR perform worse than MSH-LLM, showing the effectiveness of the logical reasoning prompts and time series reasoning correlated prompts, respectively.

Table 23: The results of different logical thinking prompts.

No.	Category	Template	MAE Results
1	Instructive	Think it step by step.	**0.450**
2		Predict the outcome step by step.	0.452
3	Misleading	Use your imagination to think the results.	0.462
4		Don't think, just feel.	0.464
5	Irrelevant	She is beautiful.	0.456
6		I am hungry.	0.453

Logical Thinking Prompts. It has been shown that logical thinking prompts can significantly enhance the reasoning abilities of LLMs (Zhou et al., 2023b), especially for zero-shot and few-shot learning. To investigate the effect of different logical thinking prompts, we design seven different logical thinking prompts with three categories, i.e., instructive, misleading, and irrelevant categories. The experimental results for few-shot learning with 10% training data are shown in Table 23. The experiment is conducted on ETTh1 dataset with the forecasting length $H = 96$. The experimental results indicate that the performance is improved if we let LLMs think in a step-by-step manner. In contrast, the prompts that belong to misleading or irrelevant categories can decrease the performance of LLMs. It remains an open question how to automatically create better prompts for time series analysis.

I VISUALIZATION

Visualization of The Weight Between Text Prototypes and Word Embeddings. To investigate whether different text prototypes possess explicit semantic meanings, we conduct qualitative analysis by visualizing the similarity scores between 10 randomly selected text prototypes and word embeddings derived from 3 different word sets. The visualization results on ETTh1 dataset are given in Figure 8. From Figure 8, we can discern the following tendencies: 1) Prototypes 2, 3, 7, and 8 exhibit strong associations with word set 1 (noun-like time series descriptions), while prototypes 0, 1, and 4 show strong correlations with word set 2 (adjective-like time series descriptions). This suggests that the prototypes capture different semantic roles, indicating explicit semantic differentiation. 2) Although both word set 1 and word set 3 consist of noun-like descriptions, almost all prototypes show weak correlations with word set 3 (name-related words). The reason may be that the text prototypes encode time-series-specific, context-specific semantic information. The experimental results show that the text prototypes possess explicit meaning.

J METHOD ANALYSIS

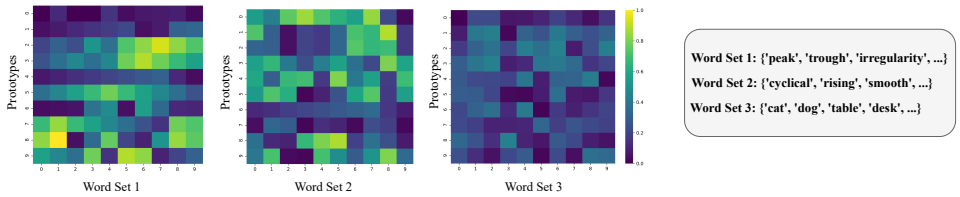

Figure 8: The visualization of the weight between text prototypes and word embeddings.

J.1 Generality Analysis on Different Tasks.

To further investigate the generalization ability of MSH-LLM across different tasks, we compare MSH-LLM with baselines in anomaly detection. Following existing works (Zhou et al., 2023a; Wu et al., 2022), we choose five commonly used datasets for comparison, including SMD (Su et al., 2019), MSL (Hundman et al., 2018), SMAP (Hundman et al., 2018), SWaT(Mathur & Tippenhauer, 2016), and PSMAbdulaal et al. (2021). The experimental seetings follow those in existing works (e.g., FPT and TimesNet). The experimental results are given in Table 24.

Table 24: The results of time series anomaly detection. We follow the protocol of existing work (Zhou et al., 2023a). The best results are **bolded**. # in the Transformers means the name of #former.

Methods	MSH-LLM	FPT	TimesNet	PatchTS#	ETS#	FED#	LightTS	DLinear	Stationary	Auto#	Pyra#	In#	Re#	LogTrans#	Trans#
SMD	88.12	86.89	84.61	84.62	83.13	85.08	82.53	77.10	84.72	85.11	83.04	81.65	75.32	76.21	79.56
MSL	84.33	82.45	81.84	78.70	85.03	78.57	78.95	84.88	77.50	79.05	84.86	84.06	84.40	79.57	78.68
SMAP	75.93	72.88	69.39	68.82	69.50	70.76	69.21	69.26	71.09	71.12	71.09	69.92	70.40	69.97	69.70
SWaT	94.58	94.23	93.02	85.72	84.91	93.19	93.33	87.52	79.88	92.74	91.78	81.43	82.80	80.52	80.37
PSM	97.45	97.13	97.34	96.08	91.76	97.23	97.15	93.55	97.29	93.29	82.08	77.10	73.61	76.74	76.07
Average	**88.08**	86.72	85.24	82.79	82.87	84.97	84.23	82.46	82.08	84.26	82.57	78.83	77.31	76.60	76.88

As shown in Table 24, MSH-LLM achieves an average F1-score of 88.08%, outperforming all baseline methods and highlighting its effectiveness in time series anomaly detection. The experimental results indicate that MSH-LLM is capable of detecting infrequent anomalies in time series, which can be attributed to the multi-scale hypergraph structure that enhances the reasoning capabilities of LLMs for modeling multi-scale temporal patterns.

J.2 Generality Analysis on Different LLM Backbones.

For a fair comparison, following existing works (Liu et al., 2024; Pan et al., 2024), we use LLaMA-7B as the default LLM backbone. However, MSH-LLM is designed to enhance the general ability of LLMs to understand and process time series data, rather than being tailored to specific LLMs (e.g., LLaMA-7B). To evaluate the performance and generality of existing methods, we evaluate MSH-LLM with other baseline methods on more advanced LLMs. We adopt LLaMA-3.1-8B (Grattafiori et al., 2024) (-w L-8B), Qwen2.5-7B (Yang et al., 2024a) (-w Q-7B), and DeepSeek-R1-Distill-LLaMA-8B (Guo et al., 2025) (-w D-8B) for comparison. The experimental results on the ETTh1 dataset with input length T=512 and output length H=96 are presented in Table 25.

Table 25: The results of different LLM backbones on ETTh1 dataset. The best results are **bolded**.

Methods	-w L-8B		-w Q-7B		-w D-8B		LLaMA-7B (Default)	
Metric	MSE	MAE	MSE	MAE	MSE	MAE	MSE	MAE
S^2IP-LLM	0.350	0.393	0.364	0.395	0.362	0.395	0.366	0.396
Time-LLM	0.378	0.403	0.379	0.413	0.378	0.408	0.383	0.410
MSH-LLM	**0.350**	**0.377**	**0.352**	**0.383**	**0.348**	**0.365**	**0.360**	**0.388**

From Table 25, we can observe that existing LLM4TS methods (i.e., MSH-LLM S^2IP-LLM, and Time-LLM) achieve better performance on more advanced LLMs, demonstrating the significance of the choice of LLM backbones for time series analysis. In addition, we can observe that MSH-LLM shows a more significant improvement compared to other methods when using more advanced LLM

backbones. This indicates the effectiveness of the framework design, rather than being merely influenced by the LLM backbones.

J.3 Robustness Analysis

All experimental results reported in the main text and appendix are averaged over three runs with different random seeds: 2021, 2022, and 2023. To evaluate the robustness of MSH-LLM to the choice of random seeds, we report the standard deviation of MSH-LLM under long-term time series forecasting settings. The experimental results are shown in Table 26 and 27. We can observe that the variances are considerably small, which indicates the robustness of MSH-LLM against the choice of random seeds.

Table 26: The standard deviation results of MSH-LLM on Weather, Electricity, and Traffic datasets. Results are averaged from three random seeds.

Dataset	Weather		Electricity		Traffic	
Horizon	MSE	MAE	MSE	MAE	MSE	MAE
96	0.138±0.0005	0.187±0.0007	0.127±0.0012	0.231±0.0005	0.365±0.0000	0.270±0.0003
192	0.187±0.0010	0.230±0.0009	0.150±0.0006	0.242±0.0003	0.372±0.0005	0.281±0.0002
336	0.237±0.0007	0.282±0.0003	0.162±0.0001	0.258±0.0000	0.385±0.0000	0.279±0.0003
720	0.305±0.0002	0.315±0.0001	0.198±0.0005	0.279±0.0003	0.402±0.0006	0.303±0.0009

Table 27: The standard deviation results of MSH-LLM on ETT dataset. Results are averaged from three random seeds.

Dataset	ETTh1		ETTh2		ETTm1		ETTm2	
Horizon	MSE	MAE	MSE	MAE	MSE	MAE	MSE	MAE
96	0.360±0.0007	0.388±0.0005	0.273±0.0009	0.331±0.0004	0.285±0.0031	0.340±0.0011	0.161±0.0001	0.246±0.0005
192	0.398±0.0014	0.411±0.0003	0.335±0.0005	0.372±0.0003	0.313±0.0016	0.358±0.0017	0.218±0.0008	0.284±0.0003
336	0.415±0.0010	0.432±0.0007	0.363±0.0007	0.400±0.0000	0.355±0.0068	0.377±0.0024	0.271±0.0005	0.320±0.0003
720	0.436±0.0003	0.447±0.0006	0.396±0.0015	0.428±0.0009	0.405±0.0121	0.410±0.0062	0.358±0.0007	0.392±0.0004

In addition, it is notable that achieving significant performance improvement across all well-studied datasets is inherently challenging. To rule out the influence of experimental errors, instead of just showing the MSE and MAE results, we repeat all experiments 3 times and report the standard deviation and statistical significance level (T-test) of MSH-LLM and the and the second-best baseline (i.e., S^2IP-LLM). The experimental results are shown in Table 28.

Table 28: The standard deviation and T-test results of MSH-LLM and the second-best baseline. Results are averaged from three random seeds.

Dataset	MSH-LLM		S^2IP-LLM		Confidence Interval
Horizon	MSE	MAE	MSE	MAE	Percent
96	0.217±0.0006	0.254±0.0005	0.223±0.0007	0.259±0.0005	99%
192	0.159±0.0006	0.253±0.0003	0.163±0.0006	0.258±0.0005	99%
336	0.381±0.0003	0.283±0.0004	0.406±0.0003	0.287±0.0004	99%
720	0.334±0.0020	0.371±0.0010	0.338±0.0014	0.379±0.0010	95%

From Table 28, we can observe that all the statistical significance reaches 95%, indicating that the performance improvements achieved by MSH-LLM are substantial and consistent across all datasets.

To evaluate the robustness of the proposed method, we compare MSH-LLM with baselines (i.e., S^2IP-LLM, Time-LLM, and FPT) across three challenging scenarios: forecasting with anomaly injection, ultra-long forecasting, and forecasting with missing data.The corresponding results are presented below.Note that to quantify robustness, we compute the performance drop rate (PDR) as:

$$PDR = \frac{\Gamma - \hat{\Gamma}}{\Gamma} \tag{18}$$

where Γ and $\hat{\Gamma}$ are forecasting results and forecasting results under challenging scenarios, respectively. Higher PDR values indicate lower robustness. The reported PDR is averaged across the MSE and MAE metrics to provide a comprehensive evaluation.

Forecasting With Anomaly Injection. We conduct experiments by injecting randomly generated anomalies in the training data. The anomaly rate varies from 10% to 20%. The experiments are conducted on ETTh1 dataset with the input length set to 512 and output length set to 96. Table 1 summarizes the results of forecasting with anomaly injection.

Table 29: Forecasting results with anomaly injection on ETTh1 dataset. The best results are **bolded**.

Methods	MSH-LLM	S^2IP-LLM	Time-LLM	FPT
Metric	MSE MAE PDR	MSE MAE PDR	MSE MAE PDR	MSE MAE PDR
0%	**0.360 0.388 /**	0.366 0.396 /	0.383 0.410 /	0.379 0.402 /
10%	**0.374 0.393 2.589**	0.712 0.574 69.743	0.398 0.419 3.056	0.410 0.393 2.970
15%	**0.425 0.427 14.053**	0.723 0.578 71.750	0.443 0.435 10.812	0.741 1.103 134.946
20%	**0.773 0.598 81.106**	0.773 0.598 81.106	0.751 0.589 69.871	0.935 1.421 200.092

From Table 29, we can obtain the following tendencies: 1) MSH-LLM achieves the best performance in almost all cases, showing its superior ability in time series forecasting even under scenarios with anomaly injection. 2) Although the performance of all methods declines as the anomaly ratio increases, MSH-LLM exhibits a slower performance degradation compared to the other methods, demonstrating its robustness for forecasting with anomaly injection. 3) When the anomaly ratio reaches about 20%, the PDR value of MSH-LLM is greater than 20%, indicating that the robustness boundary of MSH-LLM is near 20% anomaly injection.

Ultra-Long-Term Forecasting. We conduct ultra-long-term time series forecasting by taking a fixed input length (T=512) to predict ultra-long horizons (H={1008, 1440, 1800}). Table 30 summarizes the results of ultra-long-term time series forecasting.

Table 30: Ultra-long-term forecasting on ETTh1 dataset. The best results are **bolded**.

Methods	MSH-LLM	S^2IP-LLM	Time-LLM	FPT
Metric	MSE MAE	MSE MAE	MSE MAE	MSE MAE
1008	**0.463 0.498**	0.543 0.520	0.478 0.475	0.527 0.576
1440	**0.516 0.513**	0.806 0.642	0.547 0.521	0.594 0.716
1800	**0.648 0.557**	0.940 0.725	0.683 0.5587	0.660 0.886

From Table 30, we can observe that MSH-LLM achieves SOTA results on almost all cases, showing the effectiveness of MSH-LLM for ultra-long-term time series forecasting. In addition, although all baselines suffer from performance drops when increasing forecasting horizons, MSH-LLM declines more gradually. The reason may be that the multi-scale hypergraph structure enhances the ability of LLMs in understanding and processing ultra-long-term time series.

Forecasting With Missing Data.We conduct forecasting with missing data by randomly masking the training data. The experiments are conducted on Electricity dataset with the input length set to 512 and output length set to 96. Table 31 summarizes the results of forecasting with missing data.

Table 31: Ultra-long-term forecasting on ETTh1 dataset. The best results are **bolded**.

Methods	MSH-LLM	S^2IP-LLM	Time-LLM	FPT
Metric	MSE MAE	MSE MAE	MSE MAE	MSE MAE
0%	**0.360 0.388 /**	0.366 0.396 /	0.383 0.410 /	0.379 0.402 /
5%	**0.368 0.3.93 3.511**	0.385 0.403 3.479	0.392 0.416 1.907	0.392 0.431 5.307
10%	**0.409 0.421 11.058**	0.432 0.447 15.456	0.451 0.449 13.633	0.478 0.483 22.704

From Table 31, we can obtain the following tendencies: 1) Existing LLM-based methods show little performance degradation with 5% missing data. The reason may be that LLM4TS methods can leverage transferable knowledge learned from large-scale corpora of sequences, thereby enhancing their abilities in understanding and reasoning time series. 2) MSH-LLM performs better than other LLM4TS methods, the reason is that the hyperedging mechanism can capture group-wise interactions, which increase the robustness of LLM in forecasting with missing data. 3) When the missing data ratio reaches about 10%, the PDR value of MSH-LLM is greater than 10%, indicating that the robustness boundary of MSH-LLM is near 10% missing data.

J.4 Computation Cost Analysis

We compare MSH-LLM with three LLM4TS methods (i.e., S^2IP-LLM, Time-LLM, and FPT) on ETTh1 datasets with the input length of 512 and output length of 720 using a batch size of 32. It is worth noting that FPT uses GPT-2 (Radford et al., 2019) as the base LLM, while Time-LLM employs two types of base LLMs (i.e., LLaMA and GPT-2). For a fair comparison, we use GPT-2 as the base LLM and rerun baselines under unified settings to evaluate the computational complexity. The experimental results are shown in Table 32. We can observe that FPT has the fewest parameters and runs faster than other LLM4TS methods, but it gets the worst forecasting results. Compared with S^2IP-LLM and Time-LLM, although MSH-LLM has a larger number of parameters, it runs fastest due to the matrix sparsity strategy in the model and the optimization of hypergraph computation provided by *torch_geometry* (Bai et al., 2021). Overall, considering both the forecasting performance improvement and the computation cost, MSH-LLM demonstrates its superiority over existing methods.

Table 32: Computation cost.

Methods	Training Time	# Parameters	GPU Occupation	MSE results
MSH-LLM	0.104s	75,852,238	7,872MB	**0.451**
S^2IP-LLM	0.442s	63,636,512	9,991MB	0.459
Time-LLM	0.116s	53,441,968	5,403MB	0.460
FPT	**0.015**s	**36,209,616**	**2,632**MB	0.463

Table 33: Results compared with simple methods on ETTh1 dataset. The best results are **bolded**.

Methods	DHR-ARIMA		Repeat		PAtnn		MSH-LLM	
Metric	MSE	MAE	MSE	MAE	MSE	MAE	MSE	MAE
96	0.894	0.613	1.294	0.713	0.383	0.411	**0.360**	**0.388**
192	0.872	0.624	1.325	0.733	0.429	0.438	**0.398**	**0.411**
336	0.957	0.638	1.330	0.746	0.425	0.443	**0.415**	**0.432**

J.5 Broader Benchmark Comparison

Comparison With Other Cross-Modality Alignment (CMA) Method. It is known that TimeCMA (Liu et al., 2025a) also uses the CMA mechanism. We need to clarify that despite the shared nomenclature, the implementation and operational mechanisms of the cross-modality alignment (CMA) modules in MSH-LLM and TimeCMA are fundamentally different. Specifically, the CMA mechanism in TimeCMA operates primarily as a retrieval mechanism. Its goal is to query and extract time-series-related representations from a set of predefined, hand-crafted textual prompts. This process can be seen as a form of feature selection, where the most relevant linguistic cues are retrieved to augment the time series embeddings. In contrast, the CMA module in MSH-LLM operates primarily as an alignment and fusion mechanism. Its designed to align the multi-scale hyperedges features with multi-scale text prototypes generated from the token embeddings of LLMs. This process aims to align the modality between natural language and time series. In addition, we have included TimCMA for comparison. Note that due to its fixed prompt templates and restrictions on LLM selection, we failed to rerun TimeCMA under the unified settings. For a fair comparison, we reran MSH-LLM using the same settings as TimCMA. The experimental results on ETTh1 dataset with the input length T=96 are shown in Table 34.

From Table 34, we can observe that MSH-LLM performs better than TimeCMA in almost all cases, demonstrating the effectiveness of CMA mechanism used in MSH-LLM.

Comparison With Simple Methods. Recent studies have questioned the effectiveness of previous LLM-based methods for time series analysis (Tan et al., 2024). Some studies even show that a simple attention layer or non-neural methods (Hewamalage et al., 2023) can achieve comparable performance. To further evaluate the performance of MSH-LLM against simple methods, we add three simple methods, i.e., PAtnn (Tan et al., 2024), DHR-ARIMA (Hewamalage et al., 2023), and Repeat (used in DLinear (Zeng et al., 2022)) for comparison. All experiments are run under unified settings. The experimental results on ETTh1 dataset are shown in Table 33.

Table 34: Results compared with simple methods on ETTh1 dataset. The best results are **bolded**.

Methods	TimeCMA		MSH-LLM	
Metric	MSE	MAE	MSE	MAE
96	0.373	**0.391**	**0.362**	0.393
192	0.427	0.421	**0.417**	**0.416**
336	0.458	0.448	**0.420**	**0.423**

From Table 33, we can observe that MSH-LLM performs better than simple methods in most cases. Specifically, MSH-LLM reduces the MSE errors by 56.89%, 70.31%, and 5.20% compared to DHR-ARIMA, Repeat, and PAtnn, respectively. The experimental results demonstrate the effectiveness of MSH-LLM over simple methods.

Here, we attribute the limited effectiveness of previous LLM-based methods for time series analysis to three key factors: Firstly, the semantic spaces of natural language and time series are inherently different. Existing methods (e.g., FPT (Zhou et al., 2023a)) directly leverage off-the-shelf LLMs for time series analysis without proper alignment, making it difficult for LLMs to understand and process temporal features. Secondly, we found that some of these methods (e.g., CALF (Liu et al., 2025b) and FPT) do not even use prompts for LLMs, despite prompts being proven crucial for activating the reasoning capabilities of LLMs. The third and most important factor is that existing LLM-based methods directly segment the input time series into patches and feed them into LLMs. However, simple partitioning of patches may introduce noise interference and negatively impact the ability of LLMs to understand and process temporal information.

In contrast, our proposed method incorporate hyperedging mechanism, CMA module, and MoP mechanism, all of which are designed to better aligning LLMs for time series analysis. Ablation studies in Section 5.6 and Appendix H confirm that these components can enhance the ability of LLMs to understand and process temporal information. Experimental results in Appendix J.3 further validate the effectiveness of our method in both utilizing LLMs and addressing concerns about the performance ceiling of previous methods.

K PROOF

In our numerical experiments and visualization analysis, we find that different hyperedge representations capture distinct semantic information and can enhance the ability of LLMs in reasoning time series data. To further explore, we use the following theorem to characterize this behavior.

Theorem 1 (Informal). Consider the self-attention mechanism for the l-th query token. Assume that the input tokens $\boldsymbol{X}_i$ $(i = 1, 2, \ldots, n)$ have a bounded mean μ. Under mild conditions, with high probability, the output value token $\hat{\boldsymbol{X}}_i$ with high probability converges to μW_i at a rate of $\mathcal{O}(n^{-1/2})$, where W_i is the parameter matrix used to compute the value token.

This indicates that the self-attention mechanism used in LLMs can efficiently converge the output token representations to a stable mean (i.e., the representative semantic center). For time series analysis, if there are translation-invariant structures or patterns (e.g., periodicity and trend), the self-attention can help identify those invariant structures more effectively by comparing a given token with others. This phenomenon is especially important in few-shot forecasting or high-noise scenarios as it helps avoid overfitting to noise and improves generalization.

However, raw time series data suffer from two main limitations: 1) Individual time points contain limited semantic information, making it difficult to reflect structural patterns (e.g., periodicity and trend). 2) The raw sequence is often corrupted by noise, resulting in a low signal-to-noise ratio. To address these issues, we introduce multi-scale hypergraph structures, which adaptively connect multiple time points through learnable hyperedges at different scales. This method can enhance the multi-scale semantic information of time series while reducing irrelevant information interference. It provides the self-attention mechanism in LLMs with more structured input, enabling self-attention to

distinguish between temporal patterns and noise. As a result, the generalization and robustness of LLMs are improved.

We denote the i-th element of vector $\boldsymbol{X}$ as x_i, the element in the i-th row and j-th column of matrix $\mathbf{W}$ as W_{ij}, and the j-th row of matrix $\mathbf{W}$ as $\mathbf{W}_{j:}$. Furthermore, we denote the i-th hyperedge representation (token) of the input as $\mathbf{x}_i$, where $\mathbf{x}_i = \boldsymbol{X}_i$. Following existing work (Zhou et al., 2023a), before given the formal statement of the Theorem E.1, we first show the following three assumptions.

1. Each token $\mathbf{x}_i$ is a sub-Gaussian random vector with mean $\boldsymbol{\mu}_i$ and covariance matrix $(\sigma^2/d)\mathbf{I}$, for $i = 1, 2, \ldots, n$.

2. The mean vector $\boldsymbol{\mu}$ follows a discrete distribution over a finite set $\mathcal{V}$. Furthermore, there exist constants $0 < \nu_1$ and $0 < \nu_2 < \nu_4$ such that:

   a) $\|\boldsymbol{\mu}_i\| = \nu_1$,

   b) $\boldsymbol{\mu}_i^\top \mathbf{W}_Q \mathbf{W}_K^\top \boldsymbol{\mu}_i \in [\nu_2, \nu_4]$ for all i, and $|\boldsymbol{\mu}_i^\top \mathbf{W}_Q \mathbf{W}_K^\top \boldsymbol{\mu}_j| \leq \nu_2$ for all $\boldsymbol{\mu}_i \neq \boldsymbol{\mu}_j \in \mathcal{V}$.

3. The matrices $\mathbf{W}_V$ and $\mathbf{W}_Q \mathbf{W}_K^\top$ are element-wise bounded by ν_5 and ν_6, respectively. That is, $|[\mathbf{W}_V]_{ij}| \leq \nu_5$ and $|[\mathbf{W}_Q \mathbf{W}_K^\top]_{ij}| \leq \nu_6$ for all $i, j \in [d]$.

In the above assumptions, we ensure that for a given query hyperedging representation, the difference between the clustering center and noises are large enough to be distinguished. Then, we give the formal statement of Theorem 1 as follows:

Theorem 2 (formal statement of Theorem 1). Let each hyperedge representation $\mathbf{x}_i$ be a σ-subgaussian random vector with mean $\boldsymbol{\mu}_i$, and suppose all n hyperedge representations share the same query cluster center. Under the aforementioned assumptions, if $\nu_1 > 3(\psi(\delta, d) + \nu_2 + \nu_4)$, then with probability at least $1 - 5\delta$, we have:

$$\begin{aligned}
&\left\| \frac{\sum_{i=1}^n \exp\left(\frac{1}{\sqrt{d}} \mathbf{x}_i \mathbf{W}_Q \mathbf{W}_K^\top \mathbf{x}_l^\top\right) \mathbf{x}_i \mathbf{W}_V}{\sum_{j=1}^n \exp\left(\frac{1}{\sqrt{d}} \mathbf{x}_j \mathbf{W}_Q \mathbf{W}_K^\top \mathbf{x}_l^\top\right)} - \boldsymbol{\mu}_l \mathbf{W}_V \right\|_\infty \\
&\leq 4 \exp\left(\frac{\psi(\delta, d)}{\sqrt{d}}\right) \sigma \nu_5 \sqrt{\frac{2}{dn} \log\left(\frac{2d}{\delta}\right)} \\
&\quad + 7 \left[\exp\left(\frac{\nu_2 - \nu_4 + \psi(\delta, d)}{\sqrt{d}}\right) - 1\right] \|\boldsymbol{\mu}_l \mathbf{W}_V\|_\infty,
\end{aligned}$$

where $\psi(\delta, d) = 2\sigma\nu_1\nu_6\sqrt{2\log\left(\frac{1}{\delta}\right)} + 2\sigma^2\nu_6 \log\left(\frac{d}{\delta}\right)$.

Proof. See the proof of Lemma 2 in (Wang et al., 2022) with $k_1 = k = n$.

L Limitations and Future Work

In the future, we will extend our work in the following directions. Firstly, due to our CMA module perform multi-scale alignment in a fully learnable manner, it is interesting to introduce a constraint mechanism to further enhance the alignment between multi-scale temporal features and multi-scale text prototypes. Secondly, compared to natural language processing and computer vision, time series analysis has access to fewer datasets, which may limit the expressive power of the models. Therefore, in the future, we plan to compile larger datasets to validate the generalization capabilities of our models on more extensive data.

M Use of LLMs

The authors use LLM solely as a general-purpose assistive tool for grammar and format refinement. LLM does not contribute to research ideation or experimental design. The authors take full responsibility for the content of this paper.